Photo-Rechargeable Li-Ion Batteries: Device Configurations, Mechanisms, and Materials

Akshaykumar D. Salunke,[§,1] Shubham Chamola,[§,1] Angus Mathieson,[2] Buddha Deka Boruah,[2,3] Michael de Volder,[*,2] and Shahab Ahmad[*,1]

[1]Advanced Energy Materials Group, Department of Physics, Indian Institute of Technology Jodhpur, 342037 Jodhpur, Rajasthan, India

[2]Department of Engineering, University of Cambridge, Cambridge CB3 0FS, United Kingdom

[3]Institute for Materials Discovery, University College London, WC1E 7JE, United Kingdom

[§]A.D.S. and S.C. contributed equally to this work.

Corresponding authors: Prof. Michael de Volder: Email: mfld2@cam.ac.uk

Dr. Shahab Ahmad: Email: shahab@iitj.ac.in

ABSTRACT: The development of high-performance solar cells combined with rechargeable batteries is crucial in achieving a sustainable and renewable-based energy future. Photorechargeable batteries (PRBs) are emerging dual-functionality devices, able to both harvest solar energy and store it in the form of electrochemical energy. Recently, efforts have been made in the search for advanced functional materials and integrated device configurations to improve the performance of photoenhanced batteries. A photorechargeable battery will provide a unique, standalone energy solution for self-powered remote electronic devices, independent of power grids. However, these devices currently suffer from several technical shortcomings in terms of efficiency, lifetime, and operating voltage. In this review, we present a comprehensive report on the significant research developments in the field of photo-rechargeable Li-ion batteries (Li-PRBs), including device configurations, working mechanisms, material selection, and future directions.

KEYWORDS: photorechargeable batteries, Li-ion batteries, energy storage, photovoltaics, photoconversion and storage, renewable and sustainable energy, hybrid devices, off-grid electricity

INTRODUCTION

Currently, the carbon-emitting and unsustainable fossil fuels fulfill more than 60% of global energy demand.[1,2] In 2021, the United Nations Climate Change Conference (COP26) at Glasgow (UK) has witnessed leaders and scientists from around the world reaching a consensus that, if carbon emissions are reduced by 55%, the global average temperature increment will be limited to 1.5 °C by 2030; otherwise, global temperatures could increase by 2.7 °C.[3] Therefore, concerted efforts are needed globally to replace the traditional fossil-fuel- based energy systems with renewable, environmentally friendly, and affordable systems.[4,5] Contemporary alternatives such as wind and solar power are rapidly growing sources of sustainable electricity, but their intermittency makes energy harvesting and storage, in a predictable and stable manner, a challenge. Most of these renewable energy systems need to be combined with storage systems, such as batteries, so that the electrical energy can be supplied steadily in the desired quantities and at the desired time, rather than being determined by the whims of the natural world. The extraordinary advances in battery technology over the past 20 years have resulted in a strong market penetration and increased utilization.[6] Particularly, consumer electronics and electric vehicles have spurred the development of better lithium-ion batteries (LIBs), with higher storage capacities and longer lifetimes. Such developments now make them ideal candidates for the storage and stabilization of electricity generated from renewable sources.

The first commercialized rechargeable LIB, using lithium carbon intercalation compounds, was developed in 1991 by the Japanese corporation Sony. The components of the demonstrated lithium-ion battery include lithium cobalt oxide (LiCoO2) as a cathode, graphite carbon as an anode, a polypropylene separator, and lithium hexafluorophosphate (LiPF6) in propylene carbonate and diethyl carbonate (PC/DEC = 1/1) as an electrolyte.[7] The basic device structure and the working mechanism of a typical LIB are shown in Figure 1a. Briefly, during the

discharge phase the oxidation reaction at the anode frees Li ions to travel through a liquid electrolyte solution to the cathode, which itself undergoes a reduction reaction. Meanwhile, electrons are transported through an external circuit to power a connected electronic device. For the recharge process, the redox processes reverse, and the Li ions return to the anode. In the space of two decades, LIBs have managed to occupy the majority of the battery market. Since lithium is the lightest metal and the least dense solid element with an equivalent weight of ~6.94 g mol^{-1} and a specific gravity of ~0.53 g cm^{-3}, it offers the highest theoretical specific capacity of 3860 mAh g^{-1} for the assembled LIB. [8] Lithium is also the most electropositive element, with an electrochemical potential of −3.04 V versus a standard hydrogen electrode.[9] With an energy density of 11.7 kWh kg^{-1}, lithium metal comes very close to hydrocarbons (gasoline constituents) in terms of the amount of energy it stores and can release per unit mass.[10] Solar energy is one of the most ubiquitous and easily accessible energy sources available on the surface of the earth, which can be directly converted into electrical energy using solar cells. Over the past decades, following the initial investigations into silicon semiconductors in the 1950s,[11] various new types of thin-film solar cells have been developed such as dye-sensitized solar cells (DSSCs) in early 1991 by Grätzel and O'Regan,[12] bulk heterojunction organic photo- voltaics (OPVs) in 1995 by Heeger and co-workers,[13] and perovskite solar cells (PSCs) in 2009 by Miyasaka and co-workers.[14] The basic device structure and working mechanism of a thin-film solar cell is shown in Figure 1b. Briefly, an electron−hole pair is generated by exposing a semiconductor to photons of sufficient energy to excite an electron from the valence band to the conduction band of the material. The light is coupled to the photoactive layer through a transparent conducting oxide (TCO) substrate and hole transport layer (HTL). An electron transport layer (ETL) is placed between the semiconducting photoactive layer and the metal back electrode as shown in Figure 1b, thus forming a p−i−n type solar cell. The photogenerated electrons and holes are dissociated and

move toward the ETL and HTL, respectively, due to the inbuilt potential and favorable energy landscape of the materials. Thus, both of the charge carriers, coming from different energy levels, are extracted by their respective current collectors, which results in the generation of electrical power in the external circuit.

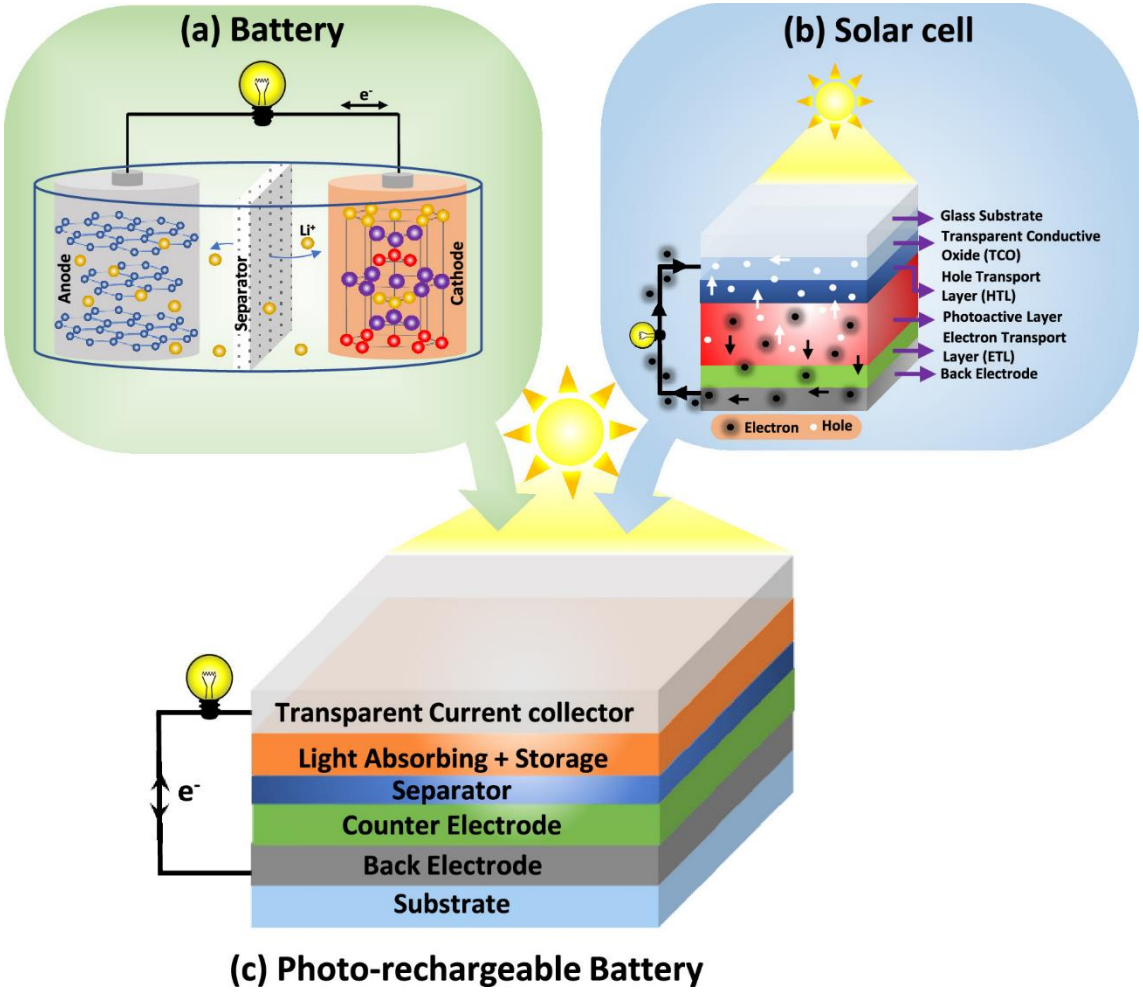

Figure 1. Schematic representations and working mechanisms of (a) a rechargeable battery and (b) a thin-film solar cell with a p−i−n junction. Note: black and white arrows in (b) indicate the directions of electron and hole movements, respectively. (c) Generalized structural representation of photorechargeable batteries.

Solar cells suffer from the intermittent nature of insolation and therefore need to be connected to energy storage systems, such as batteries, to store the electrical energy, in the form of electrochemical energy, and to stabilize their power output. Ideally, merging these two

functionalities, energy harvesting and energy storage, in a single device would significantly increase their volumetric performance and offer several other advantages. These devices are referred to as photorechargeable batteries (PRBs) or photobatteries (PBs) and are depicted in Figure 1c. Briefly, a photobattery is a single device that harvests solar energy and stores it inherently in the form of chemical energy. PBs show enhanced properties when they are exposed to light and in some cases are charged by solar energy (photocharging) without the need for an external power supply and therefore offer a unique solution for standalone remote electronic devices such as sensors, IoT (Internet of Things) devices, and sources of energy for off-grid communities. Generally, such remote electronic devices need a continuous power supply to perform sustainably and are often confined to small-device footprints. However, it is impossible to connect all these IoT devices individually or combinedly with a power source via a wired network due to their remote locations. Therefore, PRBs could be the best solution for the aforementioned issue, where each IoT device will receive a continuous power supply at all time through PRBs. Hence, on consideration of the remote nature of PRBs, which provide a unique energy solution, they may find a huge application potential to power lightweight remote sensors, IoT devices, wearable consumer electronic gadgets, smart windows, car rooftops, etc.[15−19]

In general, PBs can be classified into two broad categories: (a) three-electrode and (b) two-electrode PB configurations. Schematic representation of both configurations are shown in Figure 2. The three-electrode-configuration-based PBs are generally the physical combination of a thin-film solar cell and a LIB which uses a common electrode that is shared between the solar cell and LIB and physically separates the two devices (Figure 2a). In two-electrode PBs, the photovoltaic and LIB materials are mixed or are one and the same material. Hence, both electrodes of a two-electrode PB belong to the solar cell current collectors as well as the LIB

cathode and anode (Figure 2b,c, respectively), which allows for further size and cost reduction. The working mechanisms of these PB configurations are discussed in the subsequent sections.

On the basis of how the active material(s) are structured, two-electrode configurations can further be classified into two subcategories: (a) dual-active-material- and (b) single-active-material-based PRBs. In dual-active-material-based PBs, the absorption of solar energy and its storage in the form of electrochemical energy is being performed by two different active materials blended together; hence, both active materials perform their own functionalities but reside in the same composite. It must be noted that these different active materials can be blended together as a single electrode to form a two-electrode-type photobattery configuration as discussed above (see Figure 2b). In single-active-material-based PBs, the solar light absorption and the ion storage are performed by a single active material. Hence, this single material should have some properties of a photovoltaic solar cell (absorber layer) and a battery electrode (anode/cathode) material. In heterostructure-based PBs, two different semi-conductors are interfaced to separate the photogenerated electron−hole pair at the heterojunction efficiently (this is not shown in Figure 2); however, the energy harvesting and storage takes place in one of the semiconductors (single-active- material-based PB). In the next section, some of the recent advances in the field of three-electrode as well as two-electrode configurations with dual- and single-active-material-based PBs are discussed.

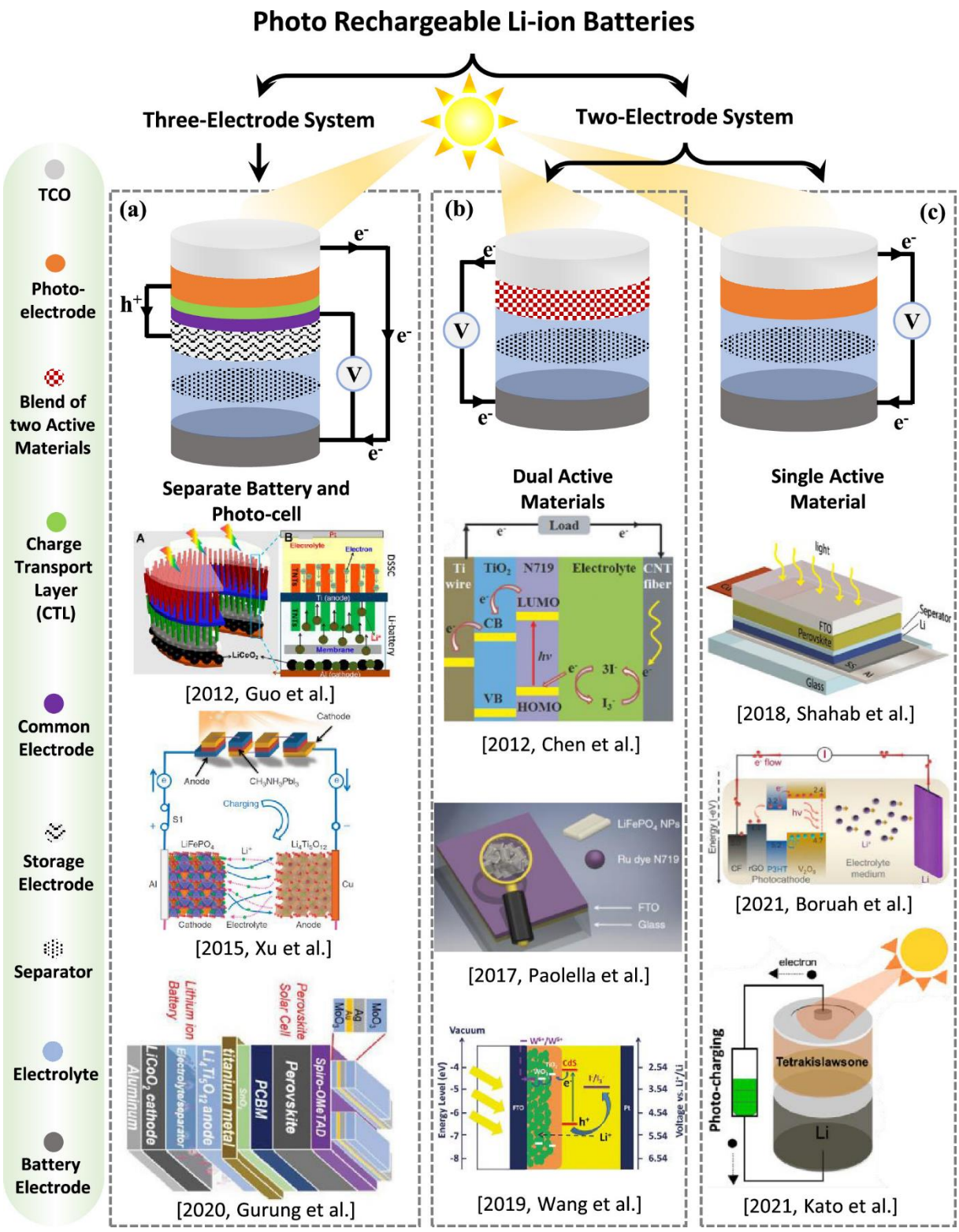

Figure 2. (a) Schematic representation of a photorechargeable battery with a three-electrode configuration, Reproduced from ref 20. Copyright 2012 American Chemical Society. Reproduced from ref 21 with permission from Springer Nature. Reproduced from ref 22 with permission from Wiley-VCH. (b) Schematic representation of a photorechargeable battery with

a two-electrode configuration with two blended active materials (photoactive and battery active). Reproduced from ref 16 with permission from Wiley-VCH. Reproduced from ref 23 with permission from Spinger Nature. reproduced from ref 24 with permission from Wiley-VCH. (c) Schematic representation of a photorechargeable battery with s twoelectrode configuration with a single active material. Reproduced from ref 25. Copyright 2018 American Chemical Society. Reproduced from ref 26. Copyright 2021 American Chemical Society. Reproduced from ref 27. Copyright 2021 American Chemical Society.

Several other PB devices based on redox flow batteries,[28–31] Na-ion,[32] K-ion,[33] and Zn-ion batteries[34–37] have also been developed in the recent past, and a few review articles have broadly described developments in the field of PBs as well as photocapacitors, redox flow batteries, and other metal-ion (Na^+, Zn^+, and Al^+) battery technologies.[38–42] However, given the industrial relevance and practical advantages of Li-ion batteries mentioned above, this review focuses only on the recent and significant developments of Li-ion based PBs by describing their classifications, device configurations, materials, and working mechanisms in detail. This review briefly sketches the evolution that PB devices have gone through recently and projects future trends and the opportunities offered by bringing the knowledge and techniques from the fields of battery and solar cell research together.

Brief History of PBs. The concept of combined solar energy harvesting and storage was first demonstrated in 1976 by Hodes et al., 188 43 where a photoelectrode, composed of a Cd−Se polycrystalline chalcogenide to absorb sunlight and an inert counter electrode (porous Ag), were submerged in an S^{2-}/S redox electrolyte solution. The photogenerated electrons at the Cd−Se photoelectrode reduced the S into S^{2-} redox species and thus an oxidation reaction between S^{2-} redox species and Ag formed Ag_2S at the porous silver counter electrode by releasing the electrons. This released electrons at the counter electrode traveled through an external load. This system stored the S^{2-} ion at the porous silver counter electrode via an

electrochemical process; thus, the system was termed a photoelectrochemical storage cell. Under AM 1.0 sunlight, the Cd−Se photoelectrode showed current and open-circuit voltages (OCV) of 7−10 mA cm^{-2} and 450−560 mV respectively. Hodes et al. also performed experiments on a three-electrode system (i.e., photoelectrode, counter electrode, and storage electrode) and revealed that the presence of all electrodes in the same electrolyte solution results in low storage efficiency and, therefore, the storage electrode needs to be separated from other electrodes by a cation-specific membrane. Additionally, it was found that the Cd−Se photoelectrode is not stable in an aqueous electrolyte due to partial S/Se substitution at the photoelectrode; thus, a great deal of research was carried out to improve the efficiency and the stability of Cd−Se photoelectrodes: for instance, Cahen et al.[44] improved the stability of the Cd−Se photoelectrode in a liquid electrolyte, by depositing a CdS layer over the Cd−Se photoelectrode using an electroplating process. Tenne et al.[45] used selective etching of the Cd−Se electrode to enhance the conversion efficiency from 2.7% to 3.6%. Following this work, Skotheim et al.[46] utilized a solvent-free polymer solid electrolyte Polyethylene oxide PEO in the system to avoid the degradation of the photoelectrode due to the aqueous electrolyte. Additionally, the interface between the photo-electrode and PEO electrolyte was modified by depositing the polypyrrole between them to transfer the charges efficiently from the photoelectrode to the redox ions of the polyethene oxide electrolyte. Finally, Licht et al.[47] improved the stability of a photoelectrochemical cell (CdSe/$[KFe(CN)_6]^{3-/2-}$) by introducing cyanide to a ferro-/ferricyanide electrolyte solution. In this system, the reaction between cyanide and ferricyanide formed cyanate, which eventually restricted the decomposition of the Cd−Se photoelectrode.

In 1981 Hada et al.[48] demonstrated a two-compartment photoelectrochemical storage cell, with titanium oxide (TiO_2) as a photoelectrode and platinum (Pt) as a counter as well as a storage electrode. The TiO_2 photoelectrode and Pt counter electrodes were immersed in an aqueous

$Ce(SO_4)_2/Ce_2(SO_4)_3$ plus HNO_3 electrolyte containing compartment, while the Pt storage electrode was immersed in an aqueous $AgNO_3$ plus KNO_3 electrolyte containing compartment. Those two compartments were separated by an anion-specific membrane and the setup was described as a solid-state photogalvanic cell. The charging of this cell was carried out by exposing the photoelectrode to ultraviolet (UV) light (300−400 nm), where the photogenerated holes at the TiO_2 photoelectrode oxidized the Ce^{3+} and electrons traveled toward the storage electrode through an external circuit. These accumulated electrons reduced the Ag^+ at the storage electrode. Therefore, the charges were stored in the solid-state electrode by oxidizing the Ce^{3+} at the photoelectrode and reducing the Ag^+ at the storage electrode. Subsequently, in 1983, Yonezawa et al.[49] used a similar experimental setup; however, they used a different photoelectrode (n-GaP) and electrolytes (aqueous $K_3[Fe\text{-}(CN)_6]/H_4[Fe(CN)_6]$ and aqueous $NiSO_4$). This system was called a photochemical storage battery. The photochemical storage battery achieved a storage efficiency of 2%. In 1986, Sharon et al.50 utilized metal phosphides (such as cobalt, iron, molybdenum, nickel, vanadium, and tungsten) as photo-electrodes for photoelectrochemical (PEC) cells with two-compartment setups, where one redox couple in the electrolyte (Ce^{3+}/Ce^{4+}) is oxidized at the photoelectrode and the other redox couple in the electrolyte (Fe3+/Fe2+) is reduced at the inert metal storage electrode during the charging process. The highest OCV of 1.11 V was found for the cell using tungsten phosphide as the photoelectrode, while the highest photo-current of 1.768 mA cm^{-2} was observed for the cell with the nickel phosphide photoelectrode.

In 1980 Tributsch et al.[56] showed that the storage of energy through a photoelectrochemical insertion reaction at the electrolyte/electrode interface is possible if the electrode is a layered semiconducting material, and then in 1987 Betz et al.[51] utilized the same concept to store the charges at layered p-type semiconductor photocathode (i.e., copper thiophosphate, Cu_3PS_4 (Eg ≈ 2.3 eV)). In this system, Pt was used as a reference electrode, a CuCl solution as an

electrolyte, and Cu wire as a counter electrode. Under illumination, the photo- cathode absorbed light and generated the photopotential at the photocathode/electrolyte interface, which was derived from the photoinsertion reaction of Cu^+ cations, via the electrolyte, to the interlayer sites of Cu_3PS_4 photocathode. Conversely, during the discharging process, Cu+ ions left the interlayer sites from the Cu_3PS_4 photocathode and plate on the Cu counter electrode. The obtained OCV and photopotential of the prepared system were 180 and 40 mV, respectively. In 1990, Kanbara et al. developed a solid-state PEC by utilizing a solid electrolyte (Ag6I6WO4) between the photoelectrode (p-type a- Si/intrinsic a-Si capped with SiOx layer) and the counter electrode, which consisted of blend of $Ag_{0.7}V_2O_5$ and Ag6I6WO4. Under illumination, i-aSi generated the e−h pairs and the photoelectrons reached the surface of SiOx and reduced Ag^+ ions to Ag atoms at the electrode−electrolyte interface. Meanwhile, photoholes traveled toward the counter electrode via an external circuit and deintercalated the Ag^+ ion from $Ag_xV_2O_5$. The demonstrated PB showed good stability even after 900 cycles with an OCV of 0.3 V.[52] Similarly, in 1995, Nomiyama et al.[53] employed layered $CuFeTe_2$ as a photocathode, lithium perchlorate ($LiClO_4$) in acetonitrile as an electrolyte, and Pt as a counter electrode to create a PEC (see Figure 3a). As a result of illumination, the photoelectrode became negatively polarized, because photoexcited electrons got trapped at the photocathode due to the unavailability of an external connection between the photoelectrode and counter electrode. Meanwhile, holes reacted with redox species at the interface of the photocathode and electrolyte. The local polarization of the photocathode served as a driving force for the intercalation of Li-ion inside the photocathode. The energy density for the system was reported to be 0.562 Wh kg^{-1},which was attributed to the intercalation of Li+ in the layered $CuFeTe_2$ photocathode, indicating the promise of Li^+ chemistries for the improvement of PB device performance. Following this work, Zou et al.[54] employed laser-deposition techniques under vacuum and a He gas environment to deposit the TiO_2 particles (n-type, Eg ≈ 3.2 eV) over a

carbon fiber network, which worked as a photoelectrode (working electrode). In this system, TiO_2 particles were used to harvest UV light from a xenon lamp. Additionally, carbon fiber was used as a counter electrode, Pt wire as a reference electrode, and $LiClO_4$ in acetonitrile as an electrolyte to create a PB device (see Figure 3a). In the case of TiO_2 particles deposited under vacuum, the photogenerated holes became accumulated on TiO_2 particles, as the photoexcited electrons traveled toward the carbon fiber due to the good interfacial contact between TiO_2 and the carbon fiber; therefore, this enabled the adsorption of the ClO_4^- ion from the electrolyte solution. However, it was found that the TiO_2 particles deposited under a vacuum environment acted as a barrier for intercalation of Li ions at the carbon fiber. On the other hand, the deposition under a He gas environment showed a poor interfacial contact between TiO_2 particles and the carbon fiber. This insulating layer restricted the movement of photoelectrons from TiO_2 particles to the carbon fiber. Thus, TiO_2 particles became negatively charged and these negatively charged TiO_2 particles adsorbed the Li^+ from the electrolyte solution, resulting in the charge cycle of the cell. Hauch et al.[57] used dye-sensitized nanocrystalline TiO_2 to absorb light and WO_3 to store the charges through an intercalation mechanism, where TiO_2 was deposited on a WO_3-TCO-glass substrate and the counter electrode was a transparent Pt layer which was deposited on the TCO-glass substrate. The electrolyte, which contained Li^+ with an I^-/I^{3-} redox couple (dissolved in propylene carbonate solvent), was used to fill up the pores of TiO_2 and WO_3 layers and the space between the two electrodes. Under illumination, the photons were absorbed by dye molecules available on the TiO_2 particles and then the photoexcited electrons moved toward WO_3 via TiO_2. Furthermore, I^- was oxidized at electrolyte/dye interface and provided the extra electrons. As this was an open circuit system, the electrons got trapped at WO_3 and therefore negative charge at WO3 acted as a driving force for the intercalation of Li ions into it. Meanwhile, during the discharging process, the electrons traveled toward the counter electrode through an external

circuit and Li ions returned to the electrolyte; additionally, I^{3-} was reduced at the counter electrode. This system managed to store 1.8 C/cm^2 of charge under an illumination intensity of 1000 W cm^{-2} for 1 h. Figure 3a summarizes these milestones and the chronology of significant early developments of various photorechargeable systems.

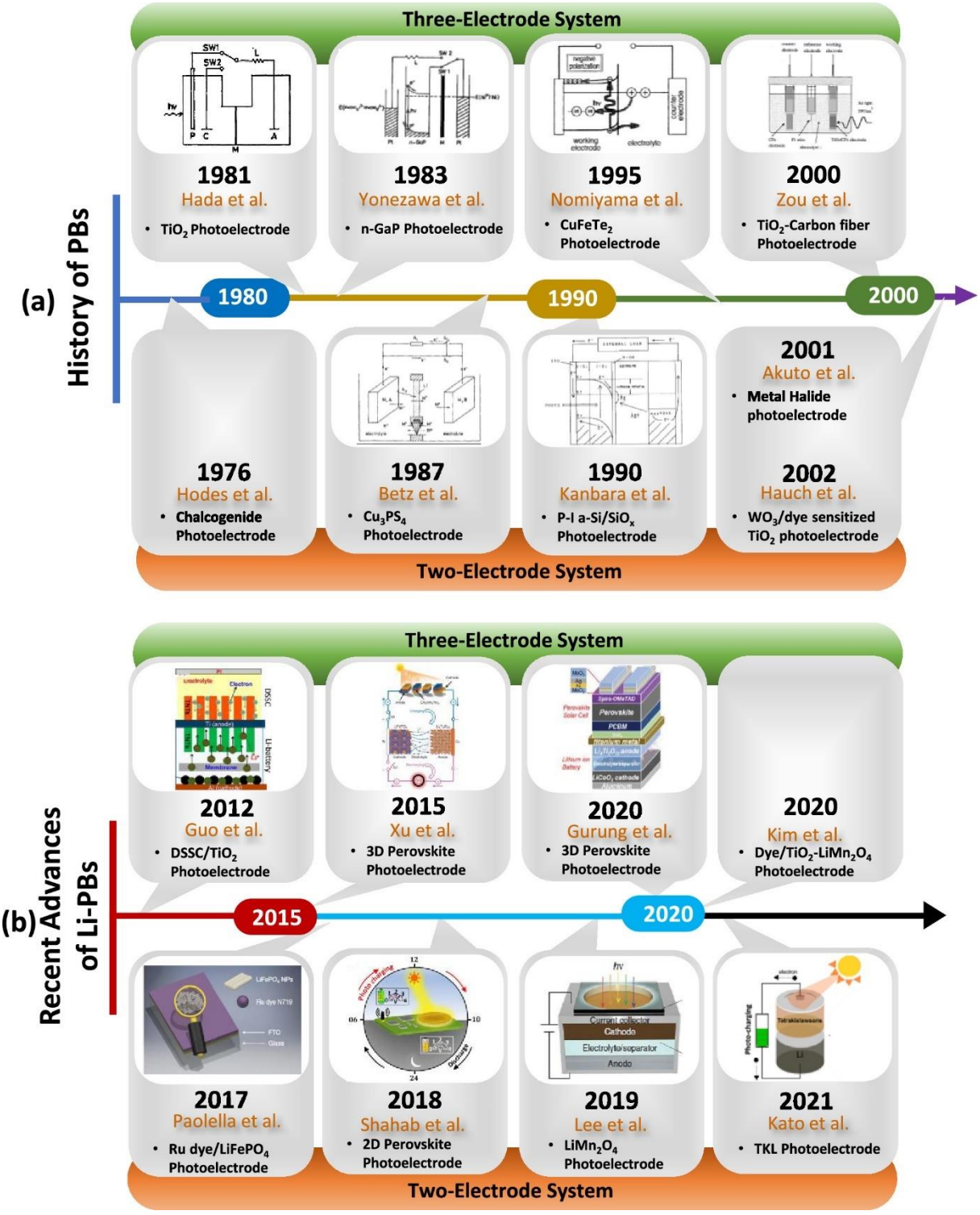

Figure 3. (a) Progress in the development of photorechargeable batteries from 1976 to 2002. Reproduced from ref 48 with permission from The Chemical Society of Japan. Reproduced from ref 49 with permission from The Chemical Society of Japan. Reproduced from ref 51 with permission from American Institute of Physics. Reproduced from ref 52 with permission from Elsevier. Reproduced from ref 53 with permission from Elsevier. Reproduced from ref 54 with permission from Elsevier. (b) The recent development of photorechargeable Li-ion batteries from 2012 to 2021. Reproduced from ref 20. Copyright 2012 American Chemical Society. Reproduced from ref 21 with permission from Springer Nature. Reproduced from ref 22 with permission from Wiley-VCH. Reproduced from ref 23 with permission from Springer Nature. Reproduced from ref 25. Copyright 2018 American Chemical Society. Reproduced from ref 55 with permission from Springer Nature. Reproduced from ref 27. Copyright 2021 American Chemical Society.

RECENT ADVANCES IN PHOTORECHARGEABLE Li-ION BATTERIES (Li-PBS)

The early work detailed above diverged into different research streams, including photorechargeable capacitors,[58,59] metal−air batteries,[60] redox-flow batteries,[61] Zn-ion batteries,[34−37] and so on. Here, we are focusing only on photorechargeable as well as photoenhanced Li-ion batteries because of their promise to yield high energy densities. As illustrated in Figure 3b, two different streams of development have taken place. First, 365 designs where the photovoltaic component and battery component share one common electrode, resulting in a three-electrode system (see Figure 2a and Figure 3b, top), are discussed. Second, we focus on two-electrode systems where the photovoltaic and battery components are blended to form a single photocathode. In 2017, Paolella and co-workers suggested a two-electrode system where photoactive dyes are mixed with a conventional LIB cathode material, and in 2018 Ahmad and co-workers presented a two-electrode system where one and the same material acts as both the light-harvesting and energy-storage material (see

Figure 3b, bottom). In addition, researchers have shown that in these two-electrode configurations light can increase the charging rate.[55] Such developments will be discussed in greater detail in the relevant sections below.

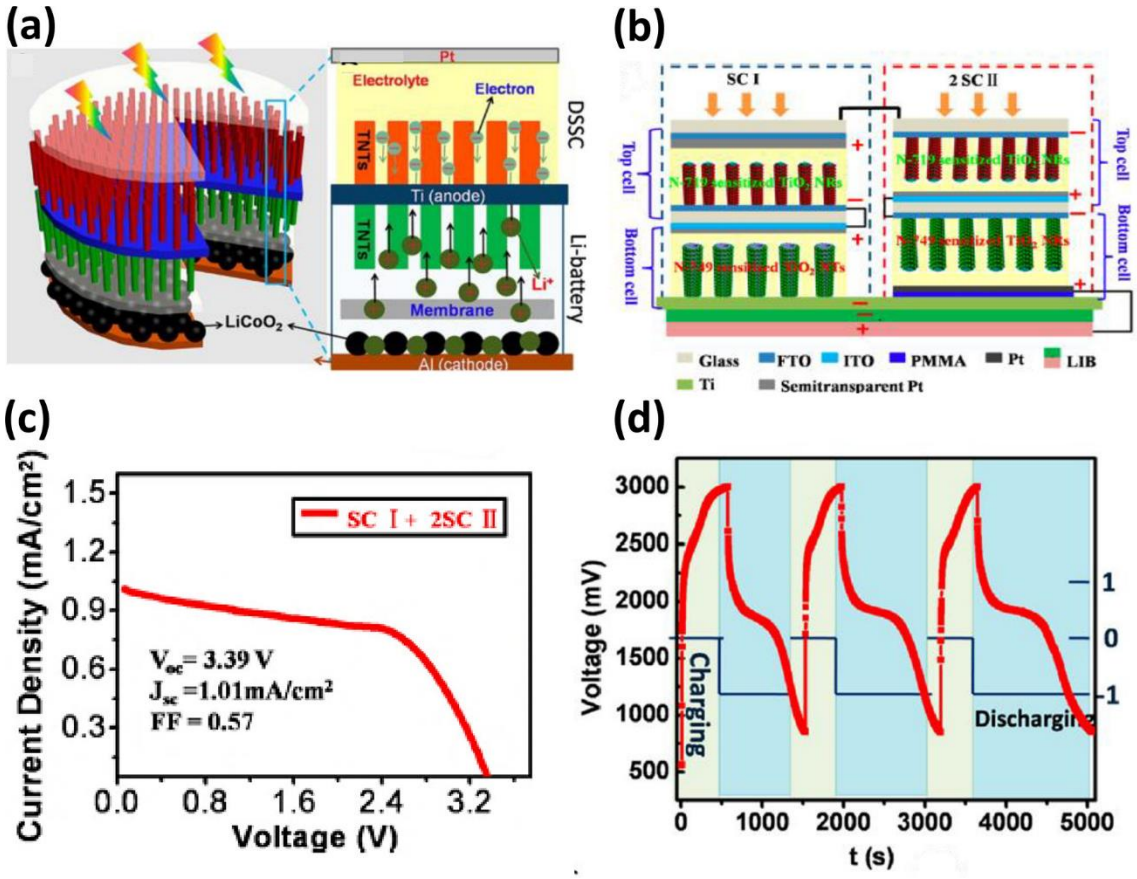

Figure 4. (a) Working principle and detailed structure of an integrated DSSC and a LIB system. (b) Detailed building blocks of three seriesconnected tandem DSSCs (i.e., SC-I and 2 SC-II) with top and bottom cells. (c) Photocurrent density−voltage (J−V) profile of three seriesconnected tandem solar cells, under an irradiation condition of 1000 W m−2 AM 1.5G. (d) Photocharge−discharge cyclic performance of integrated three series-connected tandem DSSCs and a LIB, where photocharging was carried out under irradiation of full sun intensity and discharging was carried out under a 100 μA discharge current. Reproduced from ref 20. Copyright 2012 American Chemical Society.

Three-Electrode Li-PBs. DSSC-TiO2 Nanowires for Li-PBs. The development of mesoporous structures in the photoelectrodes of DSSC has revolutionized the field of solution-processed solar cells, due to their improved light−matter interaction and coupling properties.[62−64] In 2012, Guo et al.[20] demonstrated a hybridized energy-harvesting and -storage device by integrating three tandem DSSCs and a LIB with the aid of double-side-grown vertically aligned TiO_2 nanotubes (NTs) on the titanium substrate, as shown in Figure 4a. The TiO_2 NTs were grown by using an electrochemical anodizing method. The top-side-grown TiO_2 NTs were integrated with the DSSC by sensitizing them with dye and introducing an electrolyte. The light was coupled into the solar cell through a semitransparent Pt metal electrode. The bottom-side-grown TiO_2 NTs were used as LIB anodes against $LiCoO_2$ (LCO) cathodes deposited on an Al metal foil, as shown in Figure 4a (right). To charge the LIB, three tandem solar cells were added in series to the integrated device in order to achieve sufficient output voltage to charge the battery. The building block of all three tandem solar cells consisted of two series-connected DSSCs (namely, top and bottom cells), which were sensitized by two different dyes (dye N-719 and dye N-749, respectively). The parallel connection of all three tandem solar cells was prevented by depositing poly(methyl meth-acrylate) (PMMA) over the titanium substrate (Figure 4b); thus, the Pt acted as the counter electrode for the bottom cell of the tandem solar cells.

The design used two different dyes to enable the absorption of light over a broad range of wavelengths from 400 to 550 nm by dye N719 and 600−800 nm by dye N749. The three series-connected tandem solar cells produced an OCV of ∼3.39 V, providing the potential energy required to drive the electro-chemical reaction and charge the connected LIB. As light irradiated the DSSC, the photogenerated electrons were injected from dye molecules into the conduction band of the TiO_2 layer and passed through the titanium substrate toward the anode of the LIB (bottom-side TiO_2 NTs). In a similar manner, holes accumulated at the Pt electrode.

As a result, the Li ions were reduced at the anode of the LIB by the accumulated photoelectrons and stored in the TiO_2 NTs by forming $LixTiO_2$. Figure 4c shows the J−V curve of the three series-connected tandem DSSCs, with an OCV of ∼3.39 V and Isc of ∼1.01 mA cm−2 in the presence of solar irradiation at 100 mW cm^{-2}. The photocharge−discharge curve (Figure 4d) shows that, by photocharging the device, the potential increases from 550 to 2996 mV in 440 s. The devices achieved a photoconversion and storage efficiency (PC-SE; see eq 1) of ∼0.82%.[20]

The formula for PC-SE is

$$\text{PC-SE}\ (\%) = \frac{E_{\text{discharge}}}{P_{\text{in}} \times A \times t_{\text{ch}}} \times 100 \qquad (1)$$

where $E_{discharge}$ is the discharge energy of battery (mWh), P_{in} is the input light intensity (mW cm^{-2}), A is the photovoltaic area (cm^2), and t_{ch} is the photocharging time (h).

TiO_2−Dye and $LiMn_2O_4$ for Li-PBs. Since the discovery of DSSCs, they have attracted a great deal of attention for indoor applications due to their ability to perform under diffusive light conditions.[65] In 2020, Kim et al.[66] developed a three-electrode-configuration-based Li-PB for indoor light-harvesting and -storage applications. Dye-sensitized TiO_2 particles were used as a photoelectrode (PE), lithium manganese oxide ($LiMn_2O_4$) was used as a storage electrode (SE), and a separator with one-side-deposited Pt was used as a discharge electrode (DE). An acetonitrile electrolyte with a mediator (details are mentioned below) was introduced between the PE and DE (Pt facing toward PE), thus forming a DSSC-like device architecture, whereas an acetonitrile electrolyte with $LiClO_4$ was introduced between the DE and SE to form a LIB. Under light illumination, electrons were excited in the dye molecules and transferred to the conduction band of the TiO_2. These photogenerated electrons, which traveled from the PE to the SE through an external circuit, resulted in the reduction of the $LiMn_2O_4$ at the SE (eq 2).

At the same time, the oxidation of the mediator (Mred) at the PE compartment provided the extra electrons to regenerate the photo-oxidized dye molecules (Dox) (eqs 3 and 4). These simultaneous processes (i.e., the reduction of the $LiMn_2O_4$ and regeneration of the dye molecules) continued until the complete reduction of the $LiMn_2O_4$ or complete oxidation of all mediator molecules. Conversely, during the discharge cycle, the oxidation of the reduced $LiMn_2O_4$ took place at the SE and the reduction of the oxidized mediator molecules took place at the DE in the PE compartment. Unlike the case in a DSSC, the mediators of this PB were not reduced at the counter electrode (or SE); therefore, this device was named a dye-sensitized photobattery (hereaf ter DS-PB). The redox reactions that take place at the SE and PE and in the dye molecules during photocharging are summarized below:

$$\text{At SE: } LiMn_2O_4 + Li^+ + e^- \rightarrow Li_2Mn_2O_4 \quad (2)$$

$$\text{At PE: } M_{red} \rightarrow M_{ox} + ne^- \quad (3)$$

$$D_{ox} + e^- \rightarrow D_{red} \quad (4)$$

Under both bright sunlight and dim light illumination, Kim et al. evaluated the performance of DS-PBs with three different mediators: I^-/I^{3-} (labeled 1), $Co^{2+/3+}(bpy)3$ (2), and $Cu^{+/2+}(dmp)_2$ (3) (where bpy = 2,20-bipyridine; dmp = 2,9-dimethyl-1,10-phenanthroline). These DS-PBs were photo-charged for 5 min at a light intensity of 100 mW cm^{-2}, and anincreasing trend of photocharging capacity was found for the three mediators: $Cu^{+/2+}(dmp)_2$ (38.6 C/cm^3) < $Co^{2+/3+}(bpy)_3$ (83 C/cm^3) < I^-/I^{3-} (111 C/cm^3). The effect of varying incident light intensity (Pin) and mediators on EDdCh and $\eta_{overall}$ values of the DS-PBs was discussed in the reported work, where the highest EDdCh value (7.8 mWh cm^{-3}) and ηoverall value (0.53%) at 100 mW cm^{-2} intensity were observed for the I^-/I^{3-} mediator. This was due to the dye regeneration process of the I^-/I^{3-} mediator being fast enough to contribute to the photocharging process, in comparison to the other two mediators. The lowest ηoverall value was observed for the $Cu^{+/2+}(dmp)_2$ mediator at 0.39% under the same illumination conditions.

The Coulombic efficiency (η_Q) vs discharge current density (J_{dCh}) profile shows that the η_Q value of the $Cu^{+/2+}(dmp)_2$ mediator decreases rapidly with an increasing J_{dCh} value. The reduction of ηoverall and η_Q values of the DS-PB with $Cu^{+/2+}(dmp)_2$ mediator was attributed to the slow kinetics of the dye regeneration process, which in turn limited the photocharging process or indirectly influenced the photo-triggered power generation process. It was also reported that the faster kinetics of the I^-/I^{3-} and $Co^{2+/3+}(bpy)_3$ mediators exhibited better stability and capacity retention under bright sunlight illumination, while the kinetically slow $Cu^{+/2+}(dmp)_2$ mediator showed poor capacity retention. However, under very low light intensity conditions of 0.15 mW cm^{-2}, the highest $\eta_{overall}$ value of 11.5% was observed for the $Cu^{+/2+}(dmp)_2$ mediator, because both the kinetics of dye generation via the $Cu^{+/2+}(dmp)_2$ mediator and the phototriggered power generation contributed to the photocharging process. According to the same concept, the highest light power to photoelectricity efficiency ($\eta_{IP'peak}$) at a low light intensity of <1 mW cm^{-2} was reported for the DS-PB with the $Cu^{+/2+}(dmp)_2$ mediator. Furthermore, under low light conditions, all three DS-PBs with different mediators exhibited significantly better cyclability and stability. On the basis of these results, Kim et al. concluded that the positive-potential mediator $Cu^{+/2+}(dmp)_2$ showed superior performance under indoor (low) light illumination conditions in comparison to the other two negative reduction potential mediators I^-/I^{3-} and $Co^{2+/3+}(bpy)_3$. These examples show how DSSC-based photovoltaic (PV) devices coupled with rechargeable LIB electrodes in a three-electrode configuration laid a pathway toward the development of photorechargeable LIB systems. Next, we examine the integration of contemporary photo-voltaics, such as hybrid perovskites, with LIBs to form PRBs.

Metal Halide Hybrid Perovskite Solar Cell Integrated Li-PB. Until 2015, all of the demonstrated Li-PBs showed low PC-SE values due to the low PCE of the integrated DSSCs.[20,67,68] In an attempt to improve the overall PC-SE of PBs, the PV performance of

photoelectrode is an important factor; therefore, new PV materials were employed in the PBs. To this end, metal halide perovskites (MHPs) were brought to the forefront of PBs. Over the past decade, MHPs have gained a great deal of attention for PV applications due to their outstanding optoelectronic properties such as large charge carrier mobilities ($\mu e \approx 0.2$ cm^2 V^{-1} s^{-1} and $\mu_h \approx 3.5$ cm^2 V^{-1} s^{-1} for $FAPbI_3$), large diffusion lengths (~5−10 μm), low trap state density (~10^9 to 10^{10} cm^{-3}), and optical absorbance (~10^5 cm^{-1}).[69–71] Perovskite solar cells (PSCs) have demonstrated impressively high PCEs of >25%, only within a short span of time; furthermore, their solution processability, large area scalability, and relatively low cost makes them attractive semiconductors for PVs.[72–75] The following section shows the recent attempts to combine MHP-based solar cells with LIBs to improve the overall performance of the PBs by virtue of their vastly improved PV properties.

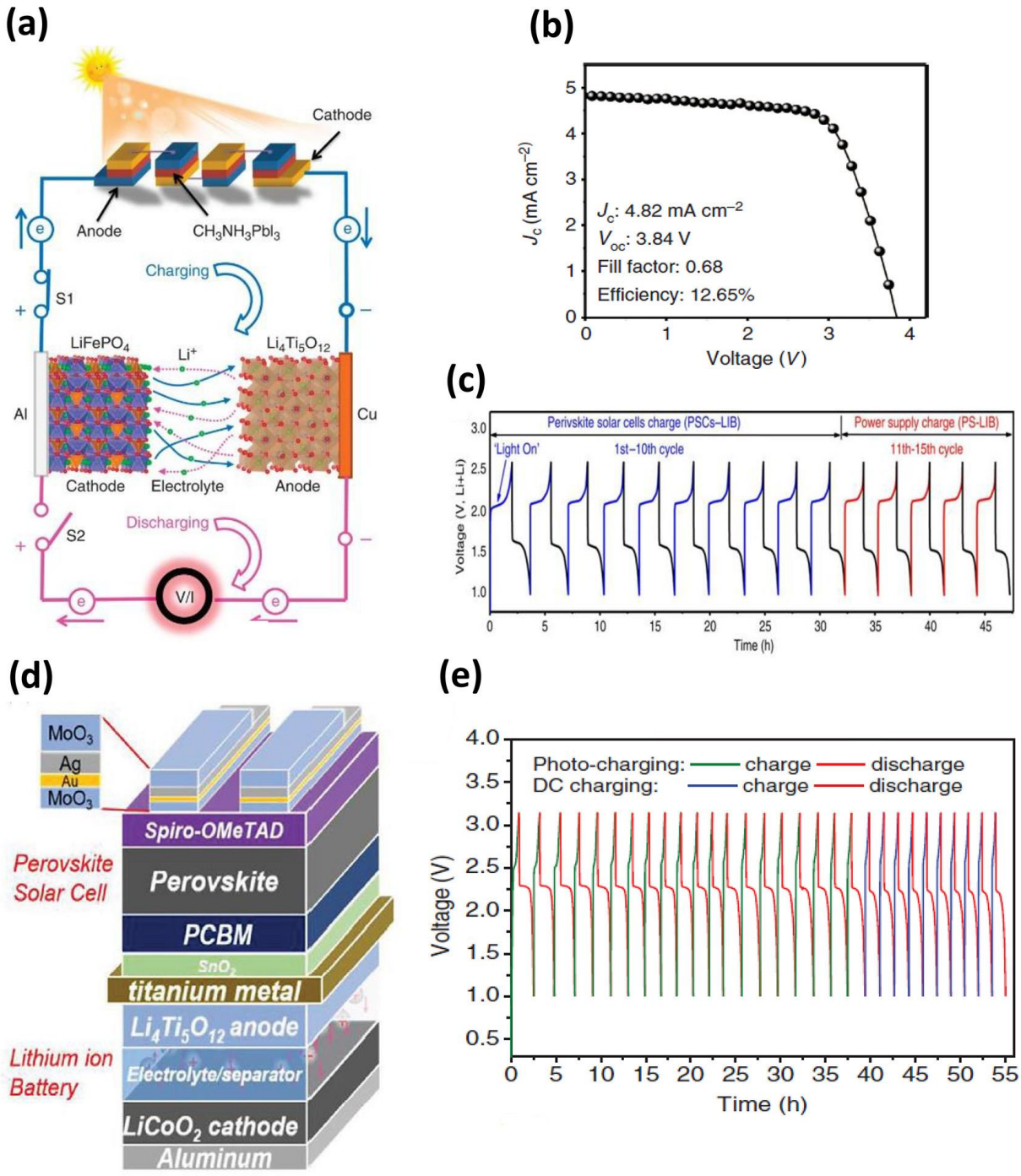

Figure 5. (a) Schematic representation and working mechanism of a LIB integrated with MHP solar cells connected in series. (b) J−V curve of four series-connected perovskite solar cells. (c) Voltage vs time curve of a MHP-assisted photorechargeable LIB: photocharging (blue lines), galvanostatic charging (red lines), and galvanostatic discharging (black lines). Reproduced from ref 21 with permission from Springer Nature. (d) Schematic representation of an integrated rear-illuminated perovskite solar cell and LIB device. (e) Charge−discharge

profile of a MHP solar-cellassisted photorechargeable LIB: photocharging (green lines), DC charging (blue lines), and DC discharging (red line). Reproduced from ref 22 with permission from Wiley-VCH.

In 2015, Xu et al. demonstrated that four perovskite solar cells (hereafter PSCs) connected in series via an external circuit can efficiently charge a LIB, thus forming an integrated Li-PB system, very similar to the case for solar-powered pocket calculators.[21] Figure 5a shows a schematic view of four $CH_3NH_3PbI_3$-based PSCs connected in series, which can generate a sufficiently high VOC to charge a Li-ion battery composed of a $LiFePO_4$ (LFP) cathode and a $Li_4Ti_5O_{12}$ (LTO) anode. Under standard 1 sun illumination, the PSCs generated VOC ≈ 3.84 V, driving the photogenerated holes and electrons move toward the LFP cathode and LTO anode, respectively, and driving the intercalation reaction of Li ions into the LTO anode. Then, during the discharging process, the electrons traveled from the anode to the cathode of the battery through an external circuit, thus returning the Li ions to the cathode through the electrolyte. The J−V curves of the four series-connected PSCs show a VOC value of ∼3.84 V, a J_{sc} value of ∼4.82 mA cm^{-2}, a fill factor of ∼0.68, and a PCE value of ∼12.65% (Figure 5b), which is exactly 4 times the V_{OC} value expected for a single PSC (∼0.96 V). The full cell, LFP-LTO, showed good rate cyclability over a wide range of C rates from 0.2 to 2 C with average charge/discharge capacities of 145.3/144.3 mAh g^{-1} at 0.2 C and 135.7/135.1 mAh g^{-1} at 0.5 C.

Figure 5c shows the photocharging and galvanostatic discharging cycles as well as the galvanostatic charge−discharge (by external power supply) cycles of the integrated PB system. The results show highly stable and identical charge−discharge curves for different charging sources, which implies that the LIB can be efficiently and reliably charged at a current density of ∼0.085 mAg^{-1} (0.5 C), which matches well with the photogenerated current density from the PSC unit over the voltage range of 2.0−2.5 V (4.61−4.52 mA cm^{-2} and 0.087−0.085 mA

g^{-1}). Moreover, these integrated Li-PBs retained 79.49% of their initial reversible capacity of 140.4 mAh g^{-1} (i.e., ∼2.05% decay per cycle) after 10 photocharging and galvanostatic discharging cycles and showed a PC-SE value of 7.80%, which is the highest for any integrated Li-PB. Under the same guise of integrating a PSC and LIB, in 2020 Gurung et al.[22] demonstrated a three-electrode Li-PB composed of a PSC with an LTO/$LiCoO_2$ (LCO) LIB. However, unlike the work of Xu et al.,[21] only one rear-illuminated PSC was used to charge the LIB by utilizing a voltage converter to charge the LIB through voltage matching. A titanium metal substrate was sandwiched between the PSC and LIB to isolate the two components from each other. Figure 5d illustrates the stacking of the PSC, titanium substrate, and LIB components of Li-PB. The triple-cation metal halide perovskite of the type Cs0.05(MA0.17FA0.83)0.95Pb(I0.83Br0.17)3 was used as the light-absorbing material along with spiro-OMeTAD (as the HTL) and phenyl-C61 butyric acid methyl ester (PCBM) (as the ETL), which demonstrated a PCE value of ∼18.35% under front illumination in a standalone device. Light was coupled to the Li-PB through the rear side of the PSC where dielectric−metal−dielectric (DMD) type finger contacts, composed of a layered structure of Au and MoO_3 (MoO_3 (10 nm)/Au (1 nm)/Ag (10 nm)/MoO_3 (40 nm)), were used. The J−V characteristic curve of the rear-illuminated PSC showed a Jsc value of 15.45 mA cm 601 −2, an OCV value of 1.09 V, and a fill factor of 0.656, while the J−V characteristic curve of the front-illuminated PSC showed an Jsc value of 23.3 mA cm^{-2}, an OCV value of 1.11 V, and a fill factor of 0.722. The lower performance of the rear-illuminated PSC might be attributed to two reasons: the DMD contact being less transparent than the contact used in the front-illuminated PSC (fluorine-doped tin oxide, FTO) and therefore reducing the amount of light incident on the MHP absorber layer and the HTL (spiro-OMeTAD) of the rear-illuminated PSC partially absorbing the UV−visible light.

Under the rear-side illumination, the device functioned as the photogenerated electrons moved toward the LTO (anode) via ETLs (PCBM/SnO2) and then the titanium substrate. At the same time, photogenerated holes moved toward the LCO (cathode) via the HTL, DMD contacts, and the voltage converter (not shown in the figure). As the current passed through the voltage converter the voltage induced by the PSC is stepped up, enabling the photocharging of the LIB by driving the intercalation reaction of the Li ions into the LTO. During the discharge cycle, the Li ions returned to the LCO after deintercalation from the LTO. As shown in Figure 5e, similar charge−discharge curves are observed for photocharging with galvanostatic discharging (20 cycles) and for galvanostatic charging with galvanostatic discharging (10 cycles). The reported galvanostatic discharge capacities of the rear-illuminated PSC after the 1st and 20th photocharging−galvanostatic discharging cycles were 155.2 and 115.1 mAh g^{-1} respectively. The three-electrode Li-PB demonstrated dis-charge capacities of 142.2 and 71.9 mAh g^{-1} at C/5 and 4C, respectively. The voltage-converter-assisted Li-PB demonstrated a PC-SE value of ∼7.3% and highly stable energy storage efficiency of ∼78.9%.

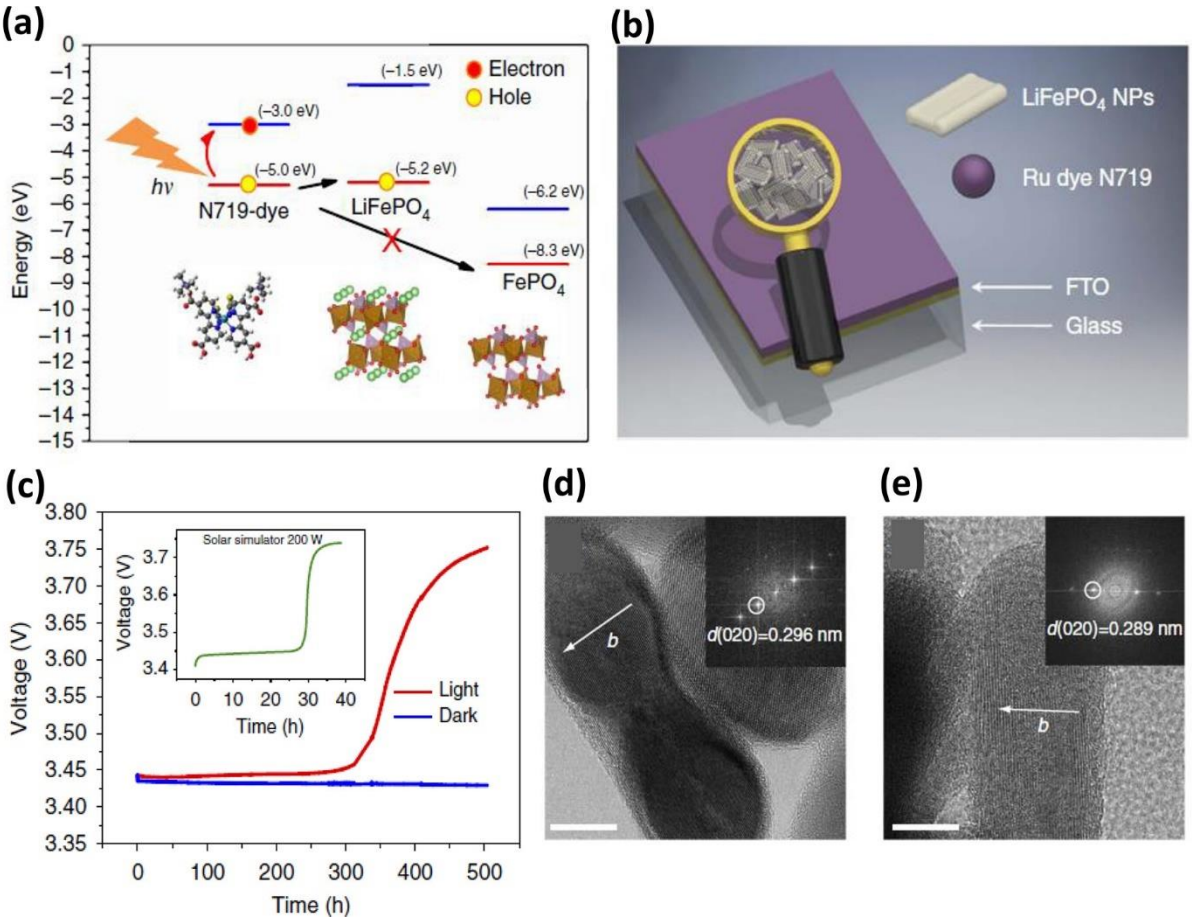

Figure 6. (a) Charge transfer process between a dye and $LiFePO_4$ electrode. (b) Schematic representation of a photocathode, fabricated by depositing N719 dye sensitized LFP nanoplatelets on an FTO substrate. (c) Variation of the OCV value with time, under a neon lamp illumination (red curve), a solar simulator illumination (green curve), and dark condition (blue curve). High-resolution TEM images of (d) the triphylite phase and (e) the heterosite phase, showing the successful Li^+ deintercalation of the $LiFePO_4$ electrode. The arrows in both images indicate the direction of Li channels. Reproduced from ref 23 with permission from Springer Nature.

Dual-Active-Material-Based Two-Electrode Li-PBs. Ru Dye−LiFePO4 Nanocomposite for Li-PBs. In addition to the integration of solar cells and LIBs, researchers have recently started working on two-electrode systems where electrodes are fabricated that are simultaneously harvesting and storing energy (see Figures 2 and 3b). In 2017 Paolella et al.[23]

suggested a new two-electrode cell design where a dye was combined with $LiFePO_4$ nanoplatelets (NPs) to form a photocathode. A ruthenium (Ru)-based N719 dye was used as a solar absorption medium; under illumination photo-generated holes traveled from the dye to the $LiFePO_4$ (cathode) (Figure 6a). The author suggested that the accumulation of photogenerated holes at the cathode surface initiated a photon-induced oxidation of the $LiFePO_4$ by releasing the Li^+ ions into the electrolyte. The released Li^+ ion accumulated at the surface of Li metal (anode), whereas the photogenerated electrons were suggested to reduce the oxygen present in the electrolyte ($LiPF_6$ in ethylene carbonate (EC), DEC, and vinylene carbonate (VC)) at cathode surface, instead of reducing the Li^+ ion at the anode surface. The reduced oxygen initiated the reactions with the carbonate content of the electrolyte and the accumulated Li^+ ions at the anode. This reaction created a new Li compound containing a solid electrolyte interface (SEI) at the anode surface without disturbing its structure. A similar light-induced reaction mechanism among photoelectrons, reduced oxygen, and the carbonate content of the electrolyte was proposed by Zhu et al.[76] and Read et al.[77] in a lithium−air battery. To characterize the newly designed Li-PB, Paolella et al. initially used FTO/$LiFePO_4$ NPs/N719 dye electrodes (Figure 6b) and tested it against a Li-metal electrode under both neon light and a Xe-lamp-based solar simulator. The results revealed that the OCV value was raised from 3.45 to 3.75 V after 500 h of neon light illumination. However, a similar increment was found for the solar simulator with a faster rate, in 30 h, as shown in Figure 6c. According to the X-ray diffraction and high-resolution transmission electron microscopy results, the photoelectrode that had not been exposed to light exhibited a triphylite phase and a lattice parameter of 0.296 nm (Figure 6d). On the other hand, the electrode that had been exposed to light possessed a heterosite phase and a lattice parameter of 0.289 nm (Figure 6e), respectively. These results imply that the photo-oxidation triggered the delithiation of the triphylite phase and created a heterosite phase. The charging and discharging performances were achieved by photocharging

the cell up to 3.62 V and then discharging it at a rate of C/24 to 2.5 V, respectively. For the first photocharge cycle, the cell was charged up to 3.62 V in ∼70 h using a solar simulator with a 200 W lamp. In the case of the second photocharge cycle, the cell was charged to 3.43 V 683 in ∼100 h and thereafter the cell took another 100 h to reach 3.62 V. The charging delay in the second cycle was attributed to the dissolution of the dye in the solvents of the electrolyte. The reported Li-PB showed a PC-SE value of 0.06−0.08%.

Similarly in 2019, Wang et al. demonstrated a dual-active-material-based Li-PB with a CdS-sensitized WO3/TiO2 layer as the photoanode, where CdS and WO3 served as a photoactive material and a Li-ion storage material, respectively (see Figure 2b). The obtained photocharging capacity (19.5 mAh g^{-1}) of this Li-PB was only 10% of the recorded capacity in the standard galvanostatic charge−discharge cell (180 mAh g^{-1} at 0.2C). After 10 charge−discharge cycles under light, the maximum voltage of Li-PB was stabilized from 0.42 to 0.4 V. Furthermore, the discharge capacity of the first cycle was 7.3 mAh cm^{-2} and that of the second cycle was 4.8 mAh cm^{-2}. According to the author, the degradation or photocorrosion of photosensitive CdS could be the reason for the observed capacity fade.[24]

Single-Active-Material-Based Two-Electrode Li-PBs. Blending of the battery and solar materials into a composite can result in the blockage of sunlight by the battery material as well as losses due to a poor interface between both materials. Moreover, in comparison to physically mixing a battery and solar material, a good match of the interfacial properties such as adhesion, wetting and solvent compatibility are needed, making the practical process of electrode fabrication difficult. Recently researchers have demonstrated the use of a single active material that can simultaneously perform both light harvesting and Li-ion storage for PB applications. However, as these materials are both light-sensitive and capable of reversibly hosting metal ions, the library of materials that are able to fulfill both requirements is limited, especially when issues are taken into account such as solvent/electrolyte compatibility and shifts in band gap as

a function of the state of charge. The following subsections show some of the recent developments in the use of a single active material for two-electrode-configuration-based Li-PBs.

Layered Metal Halide Perovskite Photocathodes for Li-PBs. In 2018, Ahmad and co-workers demonstrated the use of 2D MHPs as a single active material for Li-PB applications. Like 3D (bulk) MHPs, their 2D counterparts have also received a great deal of attention due to the large room-temperature exciton binding energy of few hundreds of millielectronvolts, structural flexibility, and improved stability under an ambient air condition and under illumination.[78−80] Layered MHPs of the type (R-NH3)2MX4 (where R is an organic group, M is a divalent metal, and X is a halide) have demonstrated interesting optoelectronic properties and tuna-bility of the optical band gap by variations in their elemental composition and stacking of inorganic−organic layers.[81−94] Additionally, MHPs have also been explored as electrode materials in energy storage applications: [95,96] for instance, in 2015 Xia et al. 736 96 introduced 3D MHPs as potential anodes for LIBs and reported specific capacities of 43.6 and 331.8 mA h g^{-1} for the CH3NH3PbI3 and CH3NH3PbBr3 perovskites, respectively. Vicente et al.[97,98] subsequently reported that an Li-ion intercalation−deintercalation process did not affect the band structure of perovskite anode materials and that the Li ions had a high diffusion coefficient ($\sim 10^{-7}$ cm^2 s^{-1}) in the bulk perovskite crystal structure.

The 2D metal halide perovskites formed an orthorhombic crystal structure that consisted of layers of corner-sharing PbX6 octahedra alternating with layers of R-NH3 cations. The alternative stacking of inorganic and organic layers formed multiple quantum wells (MQWs) that showed excitonic features at room temperature. Despite the large exciton binding energies, with the use of appropriate charge transport layers, the photogenerated charge carriers could be extracted efficiently to achieve high photocurrents from these solution-processed semiconducting MHP thin films.88 Hence, on the basis of the optoelectronic, structural, and

intercalation properties of 2D metal halide perovskites, as well as their improved structural stability over their 3D counterparts, in 2018 Ahmad et al. proposed the 2D perovskite based two electrode Li-PB, shown in Figure 7a, with a 2D lead iodide perovskite of the type (C6H9C2H4NH3)2PbI4 (hereafter CHPI) as a single-active-material-based photocathode.[25] As depicted in the energy level diagram (Figure 7b) both reduced graphene oxide (rGO) and PCBM can serve as electron transfer layers. The perovskite photocathodes were fabricated by casting a dimethylformamide solution of CHPI mixed with rGO, PCBM, and polyvinylidene difluoride (PVDF) binder on an FTO substrate, resulting in vertically aligned perovskite crystalline flakes of ~320 nm thickness which, along with other additives, formed a photocathode film with an overall height of ~8−10 μm (see Figure 7c).

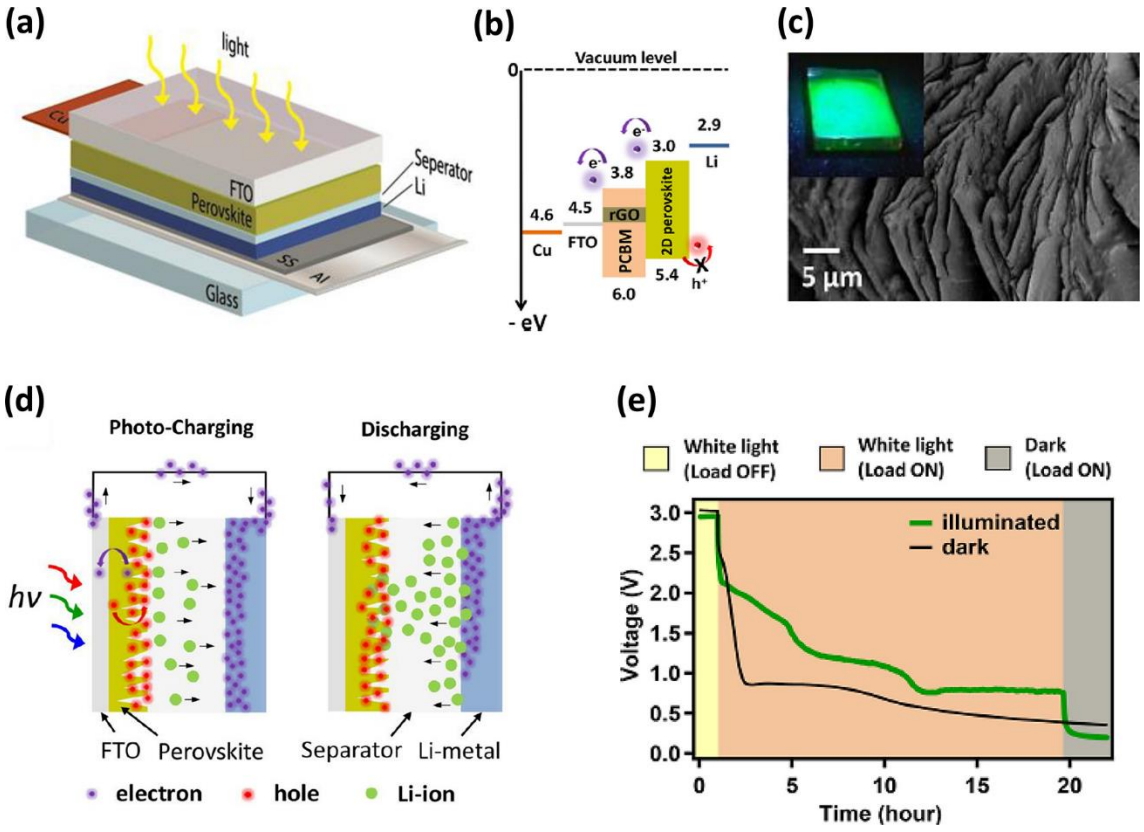

Figure 7. (a) Structural building blocks of the 2D-perovskite-based Li-PB. (b) Schematic representation of the energy levels of different materials used in the 2D-perovskite-based Li-PB. (c) SEM image and (inset) optical photograph of photoluminescence emission from the 2D

perovskite film. The photoluminescence used an LED source of λex ≈ 300 nm for excitation. (d) Visual representation of the photocharging and discharging mechanisms of a 2D-perovskite-based Li-PB. (e) Discharge voltage profile of a 2D-perovskite-based Li-PB under light ON (green curve) and light OFF (black curve) conditions. Reproduced from ref 25. Copyright 2018 American Chemical Society.

A copper foil was connected on the edge of the FTO substrate to form a current collector. The photobattery device was fabricated by assembling the perovskite photocathode, separator (soaked in 1 M LiPF6, EC/DEC 1/1 electrolyte), Li-metal electrode, and Al-foil current collector between the glass substrates, as shown in Figure 7a. In this Li-PB, the 2D perovskite acts as an active material with the dual functionality of light absorption as well as Li-ion storage. Under solar illumination, the charge transport material (rGO or PCBM) allowed photogenerated electrons to travel from the conduction band of CHPI to the copper current collector via the FTO, as shown in Figure 7b. The photoelectrons migrated toward the counter electrode (Li-metal) via an external circuit. Photogenerated holes were blocked by PCBM and thus facilitated the deintercalation of Li^+ from the perovskite photocathode to the electrolyte (Figure 7d). A similar photocharging mechanism in 2D-perovskite-based Li-PBs was also studied theoretically by He et al.,[99] where the formation of hole-polarons was attributed to the movement of Li ions during photocharging. These PBs showed a substantial capacity loss using cutoff voltages between 3.0 and 1.4 V, which could be improved by reducing the voltage window to 2.95−2.0 V. Measurements showed that under illumination the photobattery took longer to discharge from 3.0 to 1.4 V in comparison to the same PB discharged in dark conditions (Figure 7e). However, the capacity of the batteries reported in this work degraded quickly, due to stability issues of the perovskite material in the organic solvents of the liquid electrolyte. The reported perovskite-based Li-PB demonstrated a specific capacity of ∼100 mAh g^{-1} and a Coulombic efficiency of 17% for the first charge−discharge cycle; however, a

better understanding of the photocharging mechanism and Li-ion reduction by the photoelectrons at the counter electrode is required to improve the performance of these single-active material-based Li-PBs.

Furthermore, there have been several recent reports on the use of metal halide perovskites as electrode materials for LIBs: for instance, Wang et al. investigated the size-dependent performance of a methylammonium lead bromide perovskite (MAPbBr3) electrode material in a LIB. The highest cyclic stability was observed for the smallest-sized perovskite crystals of 1.2 mm, in comparison to other large-sized crystals of 1.9 and 2.9 mm, which was attributed to the fact that the smaller crystal possessed fewer defect densities and higher electrical conductivity.[100] Mathieson et al.[101] explored a Ruddlesden−Popper phase two-dimensional metal halide perovskites series of the type (BA)2(MA)n−1PbnX3n+1 (where BA is butylammonium, MA is methylammonium, and n = 1−4) for LIB anodes and achieved initial and stabilized gravimetric capacities of 575.5 and 89.9 mA h g^{-1}, respectively, for n = 4 bromide based perovskites, in addition to improving the cyclic stability of the device by the introduction of a high-molarity electrolyte (5 M of bistrifluoromethanesulfonimide lithium (LiTFSI) prepared in EC and PC solvents) chemistry.

Layered Vanadium Pentoxide (V_2O_5) Photocathodes for Li-PBs. Layered V2O5 has been explored as a potential cathode material for LIBs due to its high theoretical capacity of 294 mAh g^{-1}.[102,103] In addition, V_2O_5 is a semiconducting material having a band-gap energy range of 2.0−2.6 eV, making it suitable for Li-PB applications.[104−107] Recently, Boruah et al. reported V_2O_5-based photocathodes for Zn-ion[36] and Li-ion PBs[26] which are inspired from the aforementioned 2D perovskite Li-PBs. The photocathodes were prepared by mixing V_2O_5 nanofibers with poly(3-hexylthiophene) (P_3HT), rGO, and PVDF binder in a 91/2/2/5 ratio and drop-casted on a carbon felt current collector. This photo-cathode composition allows the generation, separation, and transportation of the photocharges to enhance Li-PBs, as illustrated

in Figure 8a. A coin cell with an optical window was used to test the photocathode against a Li-metal counter electrode in 1 M LiTFSI in EC/PC (1/1) electrolyte. As shown in Figure 8b, the discharge capacity of the Li-PB increased from ~118 to ~161 mAh g^{-1} (i.e., an ~36% capacity improvement) under illumination (455 nm wavelength, 12 mW cm^{-2} intensity) in comparison to the dark (current density 200 mA g^{-1}). It was noted that the band gap of the photocathodes changed as a function of the state of charge (SOC), as illustrated by the color changes in Figure 8c,d. It is important to note that the intercalation of Li ions into V_2O_5 moves up the Fermi level near the split-off band, which expands the energy band gap of V_2O_5.[26,108,109]

Figure 8e shows how a cell discharged under illumination stores more capacity than the same cell discharged in dark to 2.0 V. As expected from the energy level diagram (Figure 8a), the voltage of the Li-PB increased to ~2.82 V on illumination for 5 h (λ ~455 nm, intensity ~12 mW cm^{-2}). The photogenerated electrons transport from V_2O_5 into the current collector through the P3HT and rGO, due to the energetically favorable pathway. Simultaneously, the photogenerated holes increase the oxidation states of vanadium, resulting in the deintercalation of the Li ions. In addition, due to use of an inorganic active material (V_2O_5), these batteries were capable of >200 cycles, which was a great improvement over previous two-electrode-based devices. The achieved PC-SE values were ~2.6% and ~0.22% for 455 nm and 1 sun illumination, respectively.

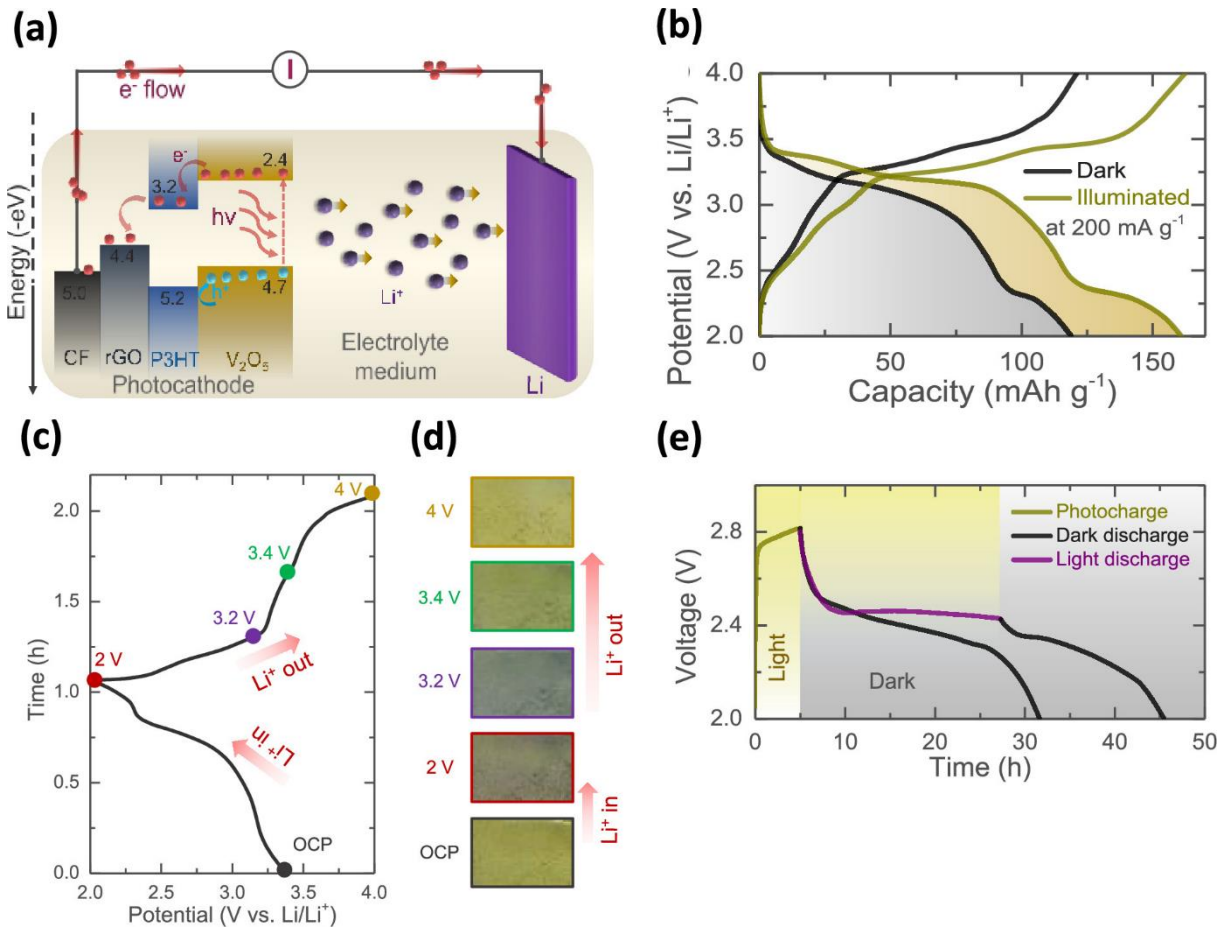

Figure 8. (a) Schematic illustration the photocharging mechanism of Li-PB composed of a layered V_2O_5 photocathode. (b) Discharge−charge profiles at 200 mA g^{-1} under dark and illuminated conditions. (c, d) Different states of charge (SOCs) of the Li-PB along with the respective images of the photocathode at the respective SOC, showing the change in color as a function of the SOC. (e) Photocharge and discharges under dark and illuminated conditions at 200 mA m^{-2}. Reproduced from ref 26. Copyright 2021 American Chemical Society.

In 2022, Wang et al. used LiV_2O_5 as a photocathode material for a two-electrode Li-PB; under the illumination, the generation of photoelectrons and oxidation of V^{4+} ions into V^{5+} ions was observed.[110] The pathways of the photoelectrons and Li ions are the same as those discussed above. The Li-ion diffusion constant was found to increase from 93.7% to 131.9%, indicating that light exposure assists the Li-ion diffusion in the charging and discharging of the PB. The obtained discharge capacity during photocharging was 185 mAh g^{-1} at 2 A g^{-1} with 5 min

charging time, which was 270% higher than the discharge capacity under dark conditions (<50 mAh g^{-1} at 2 A g^{-1}); thus, the demonstrated Li-PB had a PC-SE value of ~9%. In addition to improved Li-ion diffusion, the high crystallinity and stability of LiV_2O_5, during cyclability, was also one of the reasons for the improved performance of the demonstrated Li-PB.

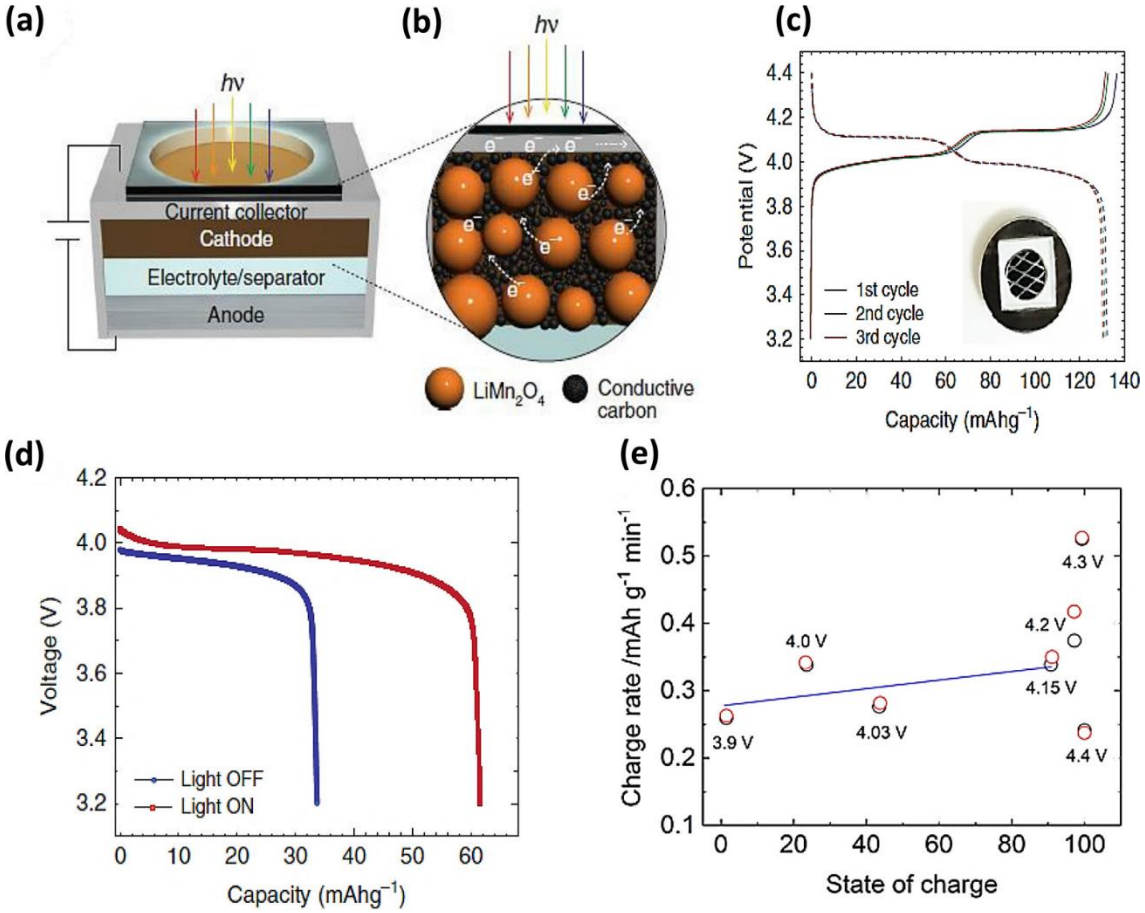

Figure 9. (a) Schematic view of an $LiMn_2O_4$-assisted Li-PRB. (b) Detailed structure of the prepared $LiMn_2O_4$ photocathode for LIB. (c) Charge− discharge profile of the prepared system between potentials of 3.2 and 4.4 V at a rate of C/10, where the solid line represents the charging process and the dashed line represents the discharging process. (d) Discharging capacity profile of an $LiMn_2O$-based Li-PRB under light ON and OFF conditions, where the

light intensity utilized for the light ON condition was 100 mW cm^{-2} (white light). (e) Charging rate of the $LiMn_2O_4$ photoelectrode with respect to the state of charge, where red and black circles represent the data obtained from two different $LiMn_2O_4$ vs Li metal coin cells. Reproduced from ref 55 with permission from Springer Nature.

$LiMn_2O_4$ Photocathodes for Li-PBs. The strategic engineering of cathode materials can help in realizing single-active material-based Li-PBs.[25] In 2019, Lee et al.[55] demonstrated the use of the most widely studied LIB cathode material, lithium manganese oxide ($LiMn_2O_4$), in Li-PBs. $LiMn_2O_4$ (LMO) cathodes are known to show a low volumetric change of ∼6% during the Li^+ insertion−disinsertion process and offer a high operating potential of ∼4 V, making them suitable as cathode materials even in a full-cell configuration.[111,112] However, it is also known that LMO cathodes exhibit capacity fading or low cyclic stability due to loss of Mn^{2+} ions to the electrolyte.[113,114] The use of an LMO-based photocathode in a Li-PB highlighted the fact that this was the first demonstration of the use of a nonconventional photovoltaic material in a PRB. The LMO had dual functionalities of light absorption and energy storage simultaneously in a two-electrode PB configuration (Figure 9a).[55] The LMO-photocathode-based Li-PRB was prepared by assembling a current collector (aluminum mesh), LMO laminate, an electrolyte (LiPF6 in EC/EMC), a glass fiber separator of grade GF/F, and lithium anode into a 2032 coin cell. Prior to coin cell assembly, an 8 mm diameter hole was punched over the upper case of the coin cell to allow light illumination on the LMO photocathode, and then that hole was sealed using Kapton tape. After all of the components were assembled in the coin cell, the Kapton tape was removed and the hole was covered using a quartz window (Figure 9b). The illumination of LMO to a standard 1 sun light source (Xe lamp 300−1100 nm) resulted in the formation of photogenerated holes (Mn^{4+}) and electrons (Figure 9b). The photogenerated electrons traveled to the counter electrode through the conducting network, current collector, and external circuit, while the photogenerated holes released Li ions from LMO into the

electrolyte. In the discharge cycle, both Li ions and electrons returned to the LMO electrode via the electrolyte and external load, respectively. A galvanostatic charge−discharge for the first three cycles of the device was performed in a reduced potential window of 3.2−4.4 V at rate of C/10 (Figure 9c), which resulted in a good capacity retention, being 90% of the theoretical capacity (133−146 mAh g^{-1}).[115] Figure 9d shows that the discharge capacity of the Li-PRB under illumination was twice that of the discharge capacity under a dark condition, implying an increase in charging rate of 3.4× under illumination. Figure 9e represents the variation of charging rate with respect to the SOC. As a result of increasing SOC values from 0% to 91%, the charging rate increased gradually (blue line). However, between 91% and 99% of the SOC, the charging rate suddenly increased and then suddenly decreased at 99% of the SOC. At the end of charge (>90% SOC), an increase in the charging rate was observed because the light-induced photocurrent provided an alternative path to reduce the charging time. On the basis of all the observations, Lee et al. proposed a mechanism by which the charging rate of the prepared PRB was improved. The generation of a large amount of Mn4+ species led to the release of an extra amount of Li ions from the LMO electrode; thus, the battery charging rate was enhanced. Finally, Lee et al. claimed that, under illumination, the LMO-based Li-PRB accelerated the charging of LIB due to an efficient charge separation process. This paper engenders an example of a Li-PRB using light to enhance the charge rate and performance of a LIB rather than causing a standalone photocharging mechanism.

Organic Photocathodes for Li-PBs. Several organic materials that are derivatives of natural products, such as derivatives of henna leaves (lawsone), have been studied for applications in batteries and solar cells,[116–119] due to their attractive properties such as Li-ion binding ability, visible light absorption (between 400 and 600 nm), low cost, and environmentally friendly nature. For example, in 2015, Khadtare et al.[119] demonstrated that lawsone-sensitized ZnO_2-based solar cells can deliver a PCE of 0.68% at a light intensity of 26 mW cm−2. In 2017 Lee

et al.[118] showed that lawsone as a cathode electrode for LIBs displayed high energy densities of up to 664 Wh kg^{-1} and discharge capacities of up to 280 mAh g^{-1} along with a capacity retention of 99%, after 1000 cycles at 0.5 C. In 2019, Miroshnikov et al.[117] utilized the tetramer of lawsone, also known as tetrakislawsone (TKL), as a cathode material in a LIB. This TKL electrode showed an initial capacity of 240 mAh g^{-1} and a capacity retention of 100 mAh g^{-1} after 300 charge−discharge cycles.

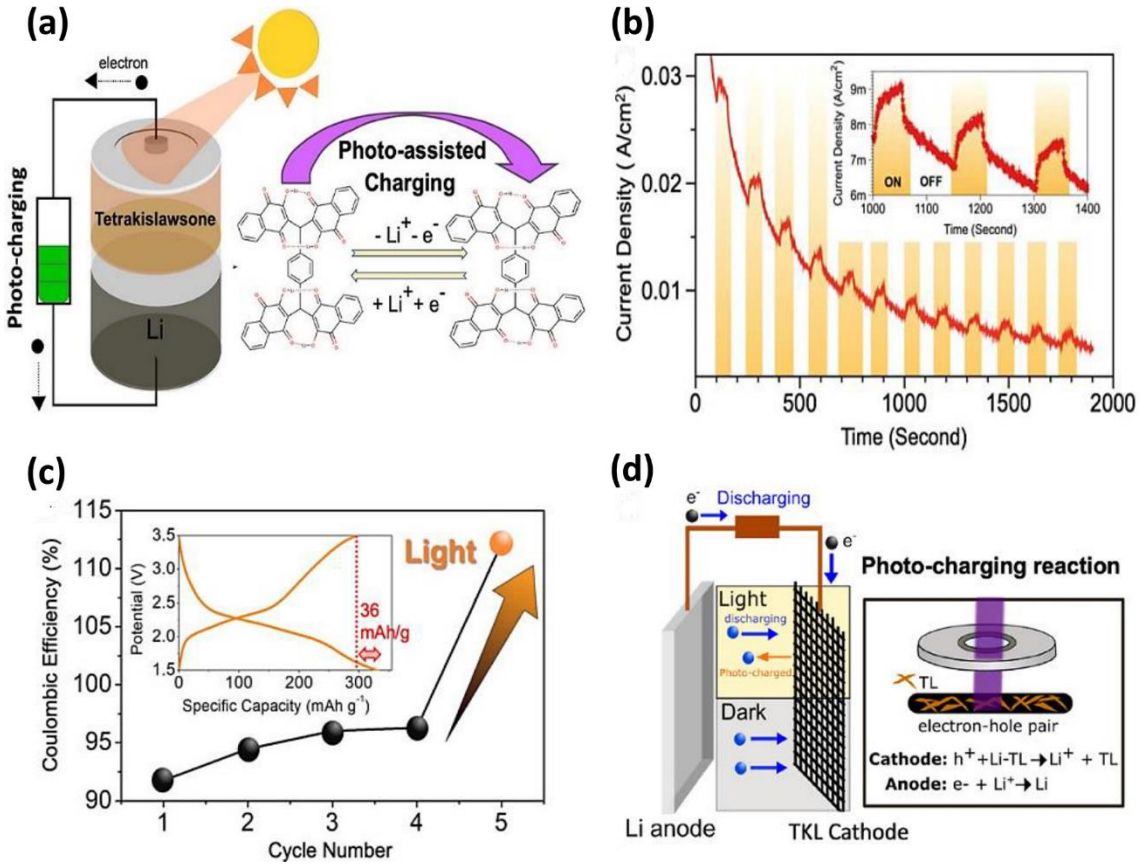

Figure 10. (a) Schematic representation of a photorechargeable TKL-based Li-PB showing the relevant oxidation and reduction processes. (b) Current density vs time profile of a TKL-based Li-PB at a constant voltage of 3 V vs Li/Li+, under light ON and OFF conditions. (c) Effect of light and dark conditions on the Coulombic efficiency of the TLK-based Li-PB. Inset: change in specific capacity for the fifth cycle. (d) Regeneration mechanism of TKL by a photocharging reaction during the discharging process. Reproduced from ref 27. Copyright 2021 American Chemical Society.

In 2021, Kato et al.[27] demonstrated an organic Li-PB by using TKL as a photocathode and Li metal as an anode. TKL, an organic semiconducting material with a direct band gap of ∼2.67 eV (unlithiated), served as the solar-absorbing layer and Li-ion storage medium. During the photocharging process, the TKL photocathode was illuminated and electron−hole pairs were generated across the band gap of the semiconductor. The authors proposed that photoexcited electrons move toward the Li-metal anode via an external circuit (Figure 10a) and photoexcited holes oxidize the lithiated TKL electrode, resulting in the extraction of the Li ions from the TKL electrode which then transfer to the Li metal via the electrolyte. During the discharge process, like other conventional LIBs, when the load was connected the electrons and Li ions spontaneously flowed from the Li anode and returned to the TKL photocathode through the external circuit and electrolyte, respectively, driven by the inherent electrochemical difference between the two electrodes. The photocharging capabilities of organic Li-PB were tested by first discharging the cell to 1.5 V (to lithiate the TKL). This stage was done, since the lithiated TKL state demonstrated a better alignment of the HOMO and LUMO with respect to the charge extraction layers in comparison to the nonlithiated TKL. Furthermore, the lithiation slightly reduced the band energy of the TKL, making it more efficient to absorb the solar energy in the ensuing photoenhanced charge and discharge stages. Next, a potential of 3 V versus Li/Li+ was applied to the cell, while it was illuminated with a 405 nm laser, to measure the increase in current. Current vs time measurements show that the current increased in the presence of laser illumination and decreased when the laser was turned off (Figure 10b). Furthermore, the charge−discharge performance of organic Li-PB was examined under light and dark conditions. The first four cycles were performed in the dark, and for the fifth cycle, the charging process was carried out in the dark and discharge was carried out under light irradiation. As a result, the discharge capacity was increased by 36 mAh g^{-1} for the fifth cycle (296 to 332 mAh g^{-1}), as shown in Figure 10c. The increase in discharge capacity for the fifth cycle was

attributed to the simultaneously competing photocharging effect during the discharge process, which regenerated the lithiated TKL back to TKL during the discharge process, as represented in Figure 10d. These organic Li-PBs did not show long cyclability; however, the predicted values of PC-SE on the basis of a theoretical estimation were reported to be around 0.68% for 26 mW cm^{-2} incident laser power and 0.58 for 100 mW cm^{-2} power, and experimentally the PC-SE was found to be 1.47% for 100 mW cm^{-2}.

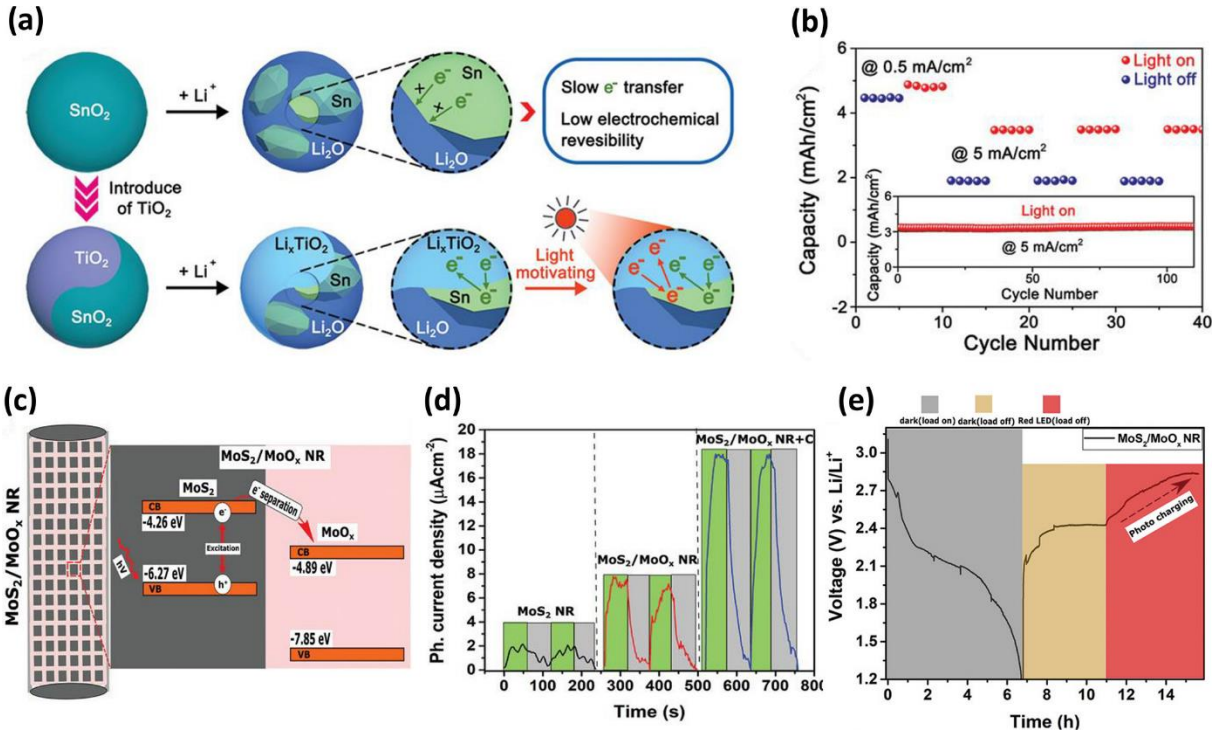

Figure 11. (a) Schematic representation of the electrochemical irreversibility and reversibility of SnO_2 in the absence and presence of TiO_2, respectively. (b) Effect of the presence and absence of light on the capacity of the fabricated photoanode at a current density of 5 mA cm^{-2}. The inset image shows the cyclic stability of photoanode for more than 100 cycles (365 nm Xe lamp with 0.025 W cm^{-2} was used for the measurement). Reproduced from ref 120 with permission from Wiley-VCH. (c) Schematic representation of fabricated MoOx/MoS2 heterojunction nanorods and their band alignment. (d) Photocurrent measurement of a MoOx/MoS2 photocathode (blue curve), MoOx/MoS_2 nanorods (red curve), and MoS2 (black

curve) under an applied bias voltage of 0.3 V vs Ag/AgCl and a power density of ∼50 mW cm^{-2}. (e) Voltage vs time curve with charging (yellow region) and discharging (black region) in dark and charging in the presence of light (red region). Reproduced from ref121 with permission from Wiley-VCH.

Heterojunction Photoelectrodes for Li-PBs. SnO_2/TiO_2 Heterojunctions. Semiconductor heterostructures have been recently introduced in Li-PBs due to their ability to efficiently separate the photogenerated electron−hole pairs in semiconductor devices. The 3D heterostructure provides maximum area for light absorption and storage of Li-ions, thus elevating the device performance. Chen et al.[120] prepared Li-PB photoelectrodes by depositing the SnO_2/TiO_2 nanoarrays onto a carbon cloth through a two-step hydrothermal process, with TiO_2 acting as both a photoactive and Li-ion-storage material. The TiO_2 nanorods acted as a core (diameter ∼200 nm), and the SnO_2 nanosheet acted as a shell (thickness ∼30 nm). The fabricated SnO_2/TiO_2 heterojunction photoanode was incorporated into a coin cell (2032) with Li foil as the counter electrode, 1 M $LiPF_6$ in 5/5 EC/ethyl methyl carbonate (EMC) as the electrolyte, and a polypropylene membrane as a separator. The PB top casing has a few holes (diameter 1 mm) through which light was irradiated on the photoelectrode. It has been observed that SnO_2 suffers from low electrochemical reversibility due to the formation of insulating LiO_2; however, the SnO_2 and TiO_2 heterostructure can partially solve this stability issue and enhance the capacity, as depicted in Figure 11a. It is proposed that, during the lithiation of TiO_2 under light illumination, the previously formed Li_xTiO_2 gets easily excited to generate e−h pairs, where due to the favorable heterojuction energy landscape the electrons were quickly transported to the SnO_2, instead of TiO_2, and thus the holes promoted the intercalation of Li+ into TiO_2 by reaching a charge balance condition. The XPS results revealed that the photogenerated electrons and holes improved the electrochemical reversibility of SnO_2 and lithiation kinetics of TiO_2, respectively. Furthermore, the performance of the SnO_2/TiO_2

photoanode was compared with those of individual SnO_2 and TiO_2 photoelectrodes. On the basis of a Tauc plot, it was concluded that the SnO_2/TiO_2 heterostructure (3.26 eV) has a band gap lower than those of TiO_2 (3.29 eV) and SnO_2 (3.74 eV). Additionally, the SnO_2/TiO_2 photoanode showed a high photoresponse (14.6 μA cm^{-2}) and fluorescence lifetime (7.39 ns) under 365 nm (Xe lamp) irradiation in comparison to TiO_2 (11.2 μA cm^{-2} and 5.2 ns), whereas no response was observed for SnO_2 under 365 nm light. The areal capacity was increased from 1.97 mAh cm^{-2} under a dark condition to 3.47 mAh cm^{-2} under a light condition, as shown in Figure 11b. Moreover, no capacity fading was observed even after 100 cycles (see inset image of Figure 11b), which was attributed to the highly stable microstructure of SnO_2/TiO_2 during cycling.

MoS_2/MoO_x Heterojunctions. Similarly in 2021, Kumar et al.[121] developed a novel MoS_2/MoO_x heterojunction photo-cathode for Li-PB by growing orthorhombic α-MoO_3 nanorods (NRs) with a diameter of 100−200 nm and length of 1−2 μm using a hydrothermal process. Further with partial sulfurization, using a chemical vapor deposition (CVD) technique, a MoS_2 interface was created over the surface of MoO_3 NRs, giving few-layer crystalline MoS_2 sheets distributed over the molybdenum mixed oxide (MoO_x) NRs. In this Li-PB, MoS_2 (2.1 eV) served as both a photoactive and Li-ion storage material. The photocathode was prepared by mixing MoO_x/MoS_2 NRs with 10% of PVDF binder and 10% of carbon black powder. Under light illumination, photogenerated electron−hole pairs get separated at the staggered heterojunction of MoO_x/MoS_2 nanorods (see Figure 11c). According to the authors, electrons traveled toward the Li anode through the MoO_x structure via an external circuit. In the meantime, accumulated holes at MoS_2 pushed Li ions into the electrolyte (1 M $LiPF_6$ in EC/EMC), which traveled toward the anode through the electrolyte and became neutralized at the anode. A comparison of the photocurrent densities of the demonstrated MoO_x/MoS_2 NRs, MoO_x/MoS_2 NRs with carbon black, and fully sulfurized MoS_2 NRs was carried out. The

heterojunction of MoO_x/MoS_2 NRs with carbon black showed the highest photocurrent density (~17 μA cm^{-2}) in comparison to MoO_x/MoS_2 NRs (8 μA cm^{-2}) and MoS_2 NRs (<2 μA cm^{-2}), which was attributed to the presence of the conducting carbon additive, as shown in Figure 11d. The demonstrated Li-PB was discharged from the attained OCV of 3.1 V to ~0.01 V with a current density of 12 mA g 1085 −1, under a dark condition (Figure 11e, black region). After a complete discharge, the battery voltage was allowed to equilibrate, which got stabilized at ~2.42 V (Figure 11e, yellow region). Next, the photocharging was carried out by illumination with red light (LED, 633 nm) with a power density of ~50 mW cm^{-2}. However, Li-PB took 4.7 h to photocharge from 2.42 to 2.83 V (Figure 11e, red region). The increase in voltage during photocharging was attributed to the delithiation of the MoO_x/MoS_2 photo-cathode. The reported discharge capacity of Li-PB under an illumination condition was 162 mAh g^{-1}, which was almost 2.3-fold higher than the discharge capacity under a dark condition; however, the lower PC-SE value (~0.05%) was attributed to the multilayer nature of MoS_2.

Table 1. Recently Developed Li-PBs with Different Two- and Three-Electrode Systems

entry	type of PB	photoactive material	storage active material	band gap of photoactive material (eV)	no. of electrodes	discharge capacity (mAh g^{-1})	PC-SE (%)	ref
1	dye-sensitized TiO_2 based Li-PB	N749 and N719 dye	TiO_2	1.4, 2.33	3	~38.89	0.82	20
2	Li-PB with $LiMn_2O_4$ as counter electrode	Y123 dye	$LiMn_2O_4$	2.01	3	~40−120		66
3	3D perovskite solar cell integrated Li-PB	$CH_3NH_3PbI_3$	$LiFePO_4$ and $Li_4Ti_5O_{12}$	1.6	3	~140.4	7.8	21
4	3D perovskite-LIB tandem based Li-PB	Cs(MAFA) Pb-$(IBr)_3$	$LiCoO_2$ and $Li_4Ti_5O_{12}$	1.62	3	~142.2−71.9	7.3	22
5	dye-sensitized $LiFePO_4$ based Li-PB	N719 dye	$LiFePO_4$	2.33	2 (dual active material)	~104	0.06−0.08	23
6	2D perovskite based Li-PB	$(C_6H_9C_2H_4NH_3)_2PbI_4$		2.4	2 (single active material)	~100	0.034	25
7	layered V_2O_5 based Li-PB	V_2O_5		2.2	2 (single active material)	~118−~161	~0.22	26
8	organic Li-PB	tetrakislawsone (organic semiconductor)		2.41 to 2.67	2 (single active material)	~296−332		27
9	MoO_x/MoS_2 heterojunction based Li-PB	MoS_2		2.1	2 (single active material)	~162	0.05	121

Material Selection Criterion and Possible Side Reactions. As three-electrode Li-PBs house the photovoltaic and battery cells sharing a common electrode, therefore the materials for three-electrode Li-PB include the ideal solar energy harvesting (PV) and energy storage (battery) materials. However, for single-active-material-based Li-PBs, in addition to the conventional energy storage properties the material must also have the following characteristics:

• The material should be ideally a direct band gap semiconductor to reduce solar energy thermalization losses.

• The material should have optical absorbance in the visible−NIR light spectrum region (400−1100 nm).

• The material should have a high absorption coefficient and large charge carrier lifetime and diffusion length.

• The conduction band minima (CBM) of the active material should match well with the energy levels/band edges of standard charge transport materials commonly used in solution processed thin-film solar cells such as PCBM, PEDOT:PSS, P_3HT, rGO, spiro-MeOTAD, TiO_2, etc. to maximize the photogenerated charge carrier extraction.

• Ideally the material should be stable in electrolyte solvents such as EC/DEC/PC/EMC/dimethyl carbonate (DMC) or aqueous systems.

• The material should be stable under a constant, potentially high intensity insolation and operating temperatures of PBs.

• The material should ideally contain nontoxic and environmentally friendly materials, to allow for sustainable development.

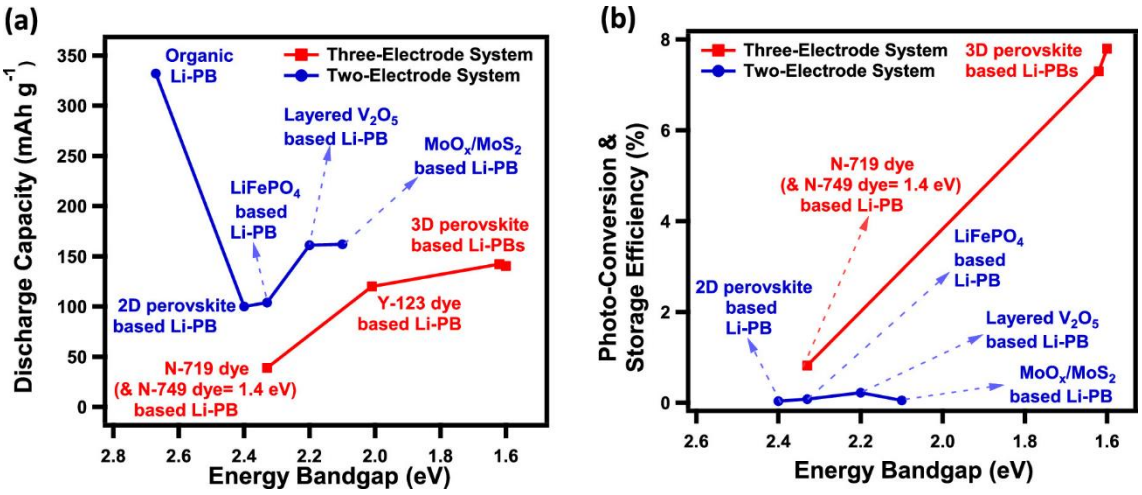

Figure 12. Variation of (a) energy band gap vs discharge capacity and (b) energy band gap vs PC-SE of various two- and three-electrode Li-PBs.

In addition to the different PB materials and configurations, it is equally important to investigate all of the possible photoassisted side reactions that may occur in PBs. For instance, electrolyte decomposition can be caused or accelerated by light interactions; while this is a field that merits more research of its own, some researchers have started to propose reaction mechanisms. On the one hand, this can be driven by reactions taking place at the material electrolyte interface. Some reports suggest that photogenerated holes can participate in the reduction of the electrolyte, similar to dye reduction in DSSC.16 On the other hand, some electrolytes themselves can degrade under illumination. In 2019, Bouteau et al.[122] investigated the influence of light irradiation (AM1.5 G) on the stability of electrolytes (1 M LiPF6 in EC/DEC) in the absence of a photoelectrode and electrode bias. The results revealed that prolonged light exposure modifies the lithium solvation by a reorganization of lithium and hexafluorophos- phate ions in the carbonates. As a result, an enhancement in the electrolyte's ionic conductivity was found (increase from 7.85 ± 0.038 to 8.32 ± 0.077 mS cm^{-1}), and a significant reduction in excited state lifetime (from 29.7 ± 0.7 to 3.2 ± 2.5 ns) was observed. However, more work is needed to understand how light affects the electrolyte performance and stability.

CONCLUSION AND OUTLOOK

PBs have been studied since the 1970s and offer an elegant solution for storing solar energy immediately and natively at the point of energy harvesting. In recent years, this has spurred the development of a range of different PB designs. This review paper focused on Li-PBs, which first found traction in three-electrode systems, where the solar cell and battery are split in different compartments that share an electrode. More recently, two-electrode designs have been proposed where the light harvesting and energy storage are combined in the same electrode. The performance parameters of these devices are summarized in Table 1.

Figure 12 indicates the main characterization metrics of light-absorbing materials against the capacity of the battery materials for recently reported two- and three-electrode Li-PBs. The PC-SE values of two-electrode Li-PBs are clearly still lower than those of three-electrode systems; nevertheless, two-electrode PBs have an advantage over three-electrode PBs, as fewer electrodes are utilized in these devices, which makes the two-electrode systems cost-effective, compact, and lightweight, which can be promising attributes of the PBs for commercialization. Further, the reduced interfaces also help in reducing the overall Ohmic transport losses in these two-electrode PRB devices. However, these devices have challenges of their own in terms of photovoltaic performance and alignment of band energies. Three-electrode PBs have better efficiencies due to the presence of a separate PV cell, which can be optimized separately and avoids electrolyte degradation by light interaction.

Despite many advances, there are still areas where further developments are required to engender efficient PBs, capable of demonstrating performance metrics that qualify their use in industrial and commercial applications. On a fundamental level, the light charging needs a better understanding; in particular, the mechanisms for charging in an open circuit and observations by several groups of charging to a voltage above those expected from the band

gap of the active material need further investigation. Practical aspects requiring more investigation include the development of better device architectures, improved large-scale manufacturing strategies, the stability of the photoactive material in the electrolyte, and the photo-stability of the electrolytes. Furthermore, the electrochemical stability of many transparent conductive electrodes and charge transport layers needs further attention to optimize the charge extraction process and therefore photocharging efficiency of the devices. In addition to the current analysis of capacity, impedance, and rate enhancement under light illumination, future work on the performance assessment would profit from a more detailed analysis of cycling stability under light/dark conditions and studies on the influence of the cutoff voltages on the PBs would be useful in order to explore their use in real device applications. Finally, as with any emerging technology, considerations must be given to the full device lifecycle, including recycling issues and the energy/cost required to make the devices, to ensure that they contribute effectively to a more sustainable global energy solution. Once they are achieved, it is evident that high-performance PBs would be a tremendous asset for further expanding our ability to harvest and store solar energy effectively.

ACKNOWLEDGMENTS

S.A. acknowledges financial support from the SERB-ECRA (ECR/2018/002056), the DST-MES (DST/TMD/MES/2K18/124G) and the DST-UKIERI (DST/INT/UK/P-167/2017). The authors are thankful to Dr. Pramod Rajput for fruitful discussions.

REFERENCES

(1) ASIF, M.; MUNEER, T. Energy Supply, Its Demand and Security Issues for Developed and Emerging Economies. Renew. Sustain. Energy Rev. 2007, 11 (7), 1388−1413.

(2) Ahmad, T.; Zhang, D. A Critical Review of Comparative Global Historical Energy Consumption and Future Demand: The Story Told so Far. Energy Reports 2020, 6, 1973−1991.

(3) United Nations Environment Programme (2021). Emissions Gap Report 2021: The Heat Is On − A World of Climate Promises Not Yet Delivered; Nairobi, 2021.

(4) Chu, S.; Majumdar, A. Opportunities and Challenges for a Sustainable Energy Future. Nature 2012, 488 (7411), 294−303.

(5) Liu, W.; McKibbin, W. J.; Morris, A. C.; Wilcoxen, P. J. Global Economic and Environmental Outcomes of the Paris Agreement. Energy Econ. 2020, 90, 104838. 1262

(6) Zhao, Y.; Pohl, O.; Bhatt, A. I.; Collis, G. E.; Mahon, P. J.; Rüther, T.; Hollenkamp, A. F. A Review on Battery Market Trends, Second-Life Reuse, and Recycling. Sustain. Chem. 2021, 2 (1), 167−205.

(7) Reddy, M. V.; Mauger, A.; Julien, C. M.; Paolella, A.; Zaghib, K. Brief History of Early Lithium-Battery Development. Materials (Basel) 2020, 13 (8), 1884.

(8) U.S. EPA Application of Life-Cycle Assessment to Nanoscale Technology: Lithium-Ion Batteries for Electric Vehicles; United States Environmental Protection Agency: 2013; pp 1−119.

(9) Liu, C.; Neale, Z. G.; Cao, G. Understanding Electrochemical Potentials of Cathode Materials in Rechargeable Batteries. Mater. Today 2016, 19 (2), 109−123.

(10) Slater, M. D.; Kim, D.; Lee, E.; Johnson, C. S. Sodium-Ion Batteries. Adv. Funct. Mater. 2013, 23 (8), 947−958.

(11) Ranabhat, K.; Patrikeev, L.; Antal'evna-Revina, A.; Andrianov, K.; Lapshinsky, V.; Sofronova, E. An Introduction to Solar Cell Technology. J. Appl. Eng. Sci. 2016, 14 (4), 481−491.

(12) O'Regan, B.; Grätzel, M. A Low-Cost, High-Efficiency Solar Cell Based on Dye-Sensitized Colloidal TiO2 Films. Nature 1991, 353 (6346), 737−740.

(13) Yu, G.; Gao, J.; Hummelen, J. C.; Wudl, F.; Heeger, A. J. Polymer Photovoltaic Cells: Enhanced Efficiencies via a Network of Internal Donor-Acceptor Heterojunctions. Science (80-.) 1995, 270 (5243), 1789−1791.

(14) Kojima, A.; Teshima, K.; Shirai, Y.; Miyasaka, T. Organometal Halide Perovskites as Visible-Light Sensitizers for Photovoltaic Cells. J. Am. Chem. Soc. 2009, 131 (17), 6050−6051.

(15) Zhang, D.; Sun, B.; Huang, H.; Gan, Y.; Xia, Y.; Liang, C.; Zhang, W.; Zhang, J. A Solar-Driven Flexible Electrochromic Supercapacitor. Materials (Basel) 2020, 13 (5), 1206.

(16) Chen, T.; Qiu, L.; Yang, Z.; Cai, Z.; Ren, J.; Li, H.; Lin, H.; Sun, X.; Peng, H. An Integrated "Energy Wire" for Both Photoelectric Conversion and Energy Storage. Angew. Chemie Int. Ed. 2012, 51 (48), 11977−11980.

(17) Chen, X.; Sun, H.; Yang, Z.; Guan, G.; Zhang, Z.; Qiu, L.; Peng, H. A Novel "Energy Fiber" by Coaxially Integrating Dye- Sensitized Solar Cell and Electrochemical Capacitor. J. Mater. Chem. A 2014, 2 (6), 1897−1902.

(18) Fu, Y.; Wu, H.; Ye, S.; Cai, X.; Yu, X.; Hou, S.; Kafafy, H.; Zou, D. Integrated Power Fiber for Energy Conversion and Storage. Energy Environ. Sci. 2013, 6 (3), 805.

(19) Zhang, Q.; Li, L.; Li, H.; Tang, L.; He, B.; Li, C.; Pan, Z.; Zhou, Z.; Li, Q.; Sun, J.; Wei, L.; Fan, X.; Zhang, T.; Yao, Y. Ultra- Endurance Coaxial-Fiber Stretchable Sensing Systems Fully Powered by Sunlight. Nano Energy 2019, 60 (March), 267−274.

(20) Guo, W.; Xue, X.; Wang, S.; Lin, C.; Wang, Z. L. An Integrated Power Pack of Dye-Sensitized Solar Cell and Li Battery Based on Double-Sided TiO 2 Nanotube Arrays. Nano Lett. 2012, 12 (5), 2520−2523.

(21) Xu, J.; Chen, Y.; Dai, L. Efficiently Photo-Charging Lithium-Ion Battery by Perovskite Solar Cell. Nat. Commun. 2015, 6 (1), 8103.

(22) Gurung, A.; Reza, K. M.; Mabrouk, S.; Bahrami, B.; Pathak, R.; Lamsal, B. S.; Rahman, S. I.; Ghimire, N.; Bobba, R. S.; Chen, K.; Pokharel, J.; Baniya, A.; Laskar, M. A. R.; Liang, M.; Zhang, W.; Zhang, W. H.; Yang, S.; Xu, K.; Qiao, Q. Rear-Illuminated Perovskite Photorechargeable Lithium Battery. Adv. Funct. Mater. 2020, 30 (30), 2001865.

(23) Paolella, A.; Faure, C.; Bertoni, G.; Marras, S.; Guerfi, A.; Darwiche, A.; Hovington, P.; Commarieu, B.; Wang, Z.; Prato, M.; Colombo, M.; Monaco, S.; Zhu, W.; Feng, Z.; Vijh, A.; George, C.; Demopoulos, G. P.; Armand, M.; Zaghib, K. Light-Assisted Delithiation of Lithium Iron Phosphate Nanocrystals towards Photo-Rechargeable Lithium Ion Batteries. Nat. Commun. 2017, 8 (1), 14643.

(24) Wang, Z.; Chiu, H.; Paolella, A.; Zaghib, K.; Demopoulos, G. P. Lithium Photo-intercalation of CdS-Sensitized WO 3 Anode for Energy Storage and Photoelectrochromic Applications. ChemSusChem 2019, 12 (10), 2220−2230.

(25) Ahmad, S.; George, C.; Beesley, D. J.; Baumberg, J. J.; De Volder, M. Photo-Rechargeable Organo-Halide Perovskite Batteries. Nano Lett. 2018, 18 (3), 1856−1862.

(26) Boruah, B. D.; Wen, B.; De Volder, M. Light Rechargeable Lithium-Ion Batteries Using V 2 O 5 Cathodes. Nano Lett. 2021, 21 (8), 3527−3532.

(27) Kato, K.; Puthirath, A. B.; Mojibpour, A.; Miroshnikov, M.; Satapathy, S.; Thangavel, N. K.; Mahankali, K.; Dong, L.; Arava, L. M. R.; John, G.; Bharadwaj, P.; Babu, G.; Ajayan, P.

M. Light-Assisted Rechargeable Lithium Batteries: Organic Molecules for Simultaneous Energy Harvesting and Storage. Nano Lett. 2021, 21 (2), 907−913.

(28) McCulloch, W. D.; Yu, M.; Wu, Y. PH-Tuning a Solar Redox Flow Battery for Integrated Energy Conversion and Storage. ACS Energy Lett. 2016, 1 (3), 578−582.

(29) Fu, H.-C.; Li, W.; Yang, Y.; Lin, C.-H.; Veyssal, A.; He, J.-H.; Jin, S. An Efficient and Stable Solar Flow Battery Enabled by a Single-Junction GaAs Photoelectrode. Nat. Commun. 2021, 12 (1), 156.

(30) Li, W.; Fu, H.-C.; Zhao, Y.; He, J.-H.; Jin, S. 14.1% Efficient Monolithically Integrated Solar Flow Battery. Chem. 2018, 4 (11), 2644−2657.

(31) Li, W.; Kerr, E.; Goulet, M.; Fu, H.; Zhao, Y.; Yang, Y.; Veyssal, A.; He, J.; Gordon, R. G.; Aziz, M. J.; Jin, S. A Long Lifetime Aqueous Organic Solar Flow Battery. Adv. Energy Mater. 2019, 9 (31), 1900918.

(32) Wang, Z.; Chiu, H.-C.; Paolella, A.; Gauvin, R.; Zaghib, K.; Demopoulos, G. P. A Sustainable Light-Chargeable Two-Electrode Energy Storage System Based on Aqueous Sodium-Ion Photo-Intercalation. Sustain. Energy Fuels 2020, 4 (9), 4789−4799.

(33) Thimmappa, R.; Paswan, B.; Gaikwad, P.; Devendrachari, M. C.; Makri Nimbegondi Kotresh, H.; Rani Mohan, R.; Pattayil Alias, J.; Thotiyl, M. O. Chemically Chargeable Photo Battery. J. Phys. Chem. C 2015, 119 (25), 14010−14016.

(34) Boruah, B. D.; Wen, B.; De Volder, M. Molybdenum Disulfide−Zinc Oxide Photocathodes for Photo-Rechargeable Zinc-Ion Batteries. ACS Nano 2021, 15 (10), 16616−16624.

(35) Boruah, B. D.; Mathieson, A.; Wen, B.; Feldmann, S.; Dose, W. M.; De Volder, M. Photo-Rechargeable Zinc-Ion Batteries. Energy Environ. Sci. 2020, 13 (8), 2414−2421.

(36) Deka Boruah, B.; De Volder, M. Vanadium Dioxide−Zinc Oxide Stacked Photocathodes for Photo-Rechargeable Zinc-Ion Batteries. J. Mater. Chem. A 2021, 9 (40), 23199−23205.

(37) Deka Boruah, B.; Mathieson, A.; Park, S. K.; Zhang, X.; Wen, B.; Tan, L.; Boies, A.; De Volder, M. Vanadium Dioxide Cathodes for High-Rate Photo-Rechargeable Zinc-Ion Batteries. Adv. Energy Mater. 2021, 11 (13), 2100115.

(38) Paolella, A.; Vijh, A.; Guerfi, A.; Zaghib, K.; Faure, C. Review Li-Ion Photo-Batteries: Challenges and Opportunities. J. Electrochem. Soc. 2020, 167 (12), 120545.

(39) Li, Q.; Liu, Y.; Guo, S.; Zhou, H. Solar Energy Storage in the Rechargeable Batteries. Nano Today 2017, 16, 46−60.

(40) Lv, J.; Xie, J.; Mohamed, A. G. A.; Zhang, X.; Wang, Y. Photoelectrochemical Energy Storage Materials: Design Principles and Functional Devices towards Direct Solar to Electrochemical Energy Storage. Chem. Soc. Rev. 2022, 51 (4), 1511−1528.

(41) Gurung, A.; Qiao, Q. Solar Charging Batteries: Advances, Challenges, and Opportunities. Joule 2018, 2 (7), 1217−1230.

(42) Zeng, Q.; Lai, Y.; Jiang, L.; Liu, F.; Hao, X.; Wang, L.; Green, M. A. Integrated Photorechargeable Energy Storage System: Next-Generation Power Source Driving the Future. Adv. Energy Mater. 2020, 10 (14), 1903930.

(43) HODES, G.; MANASSEN, J.; CAHEN, D. Photoelectrochemical Energy Conversion and Storage Using Polycrystalline Chalcogenide Electrodes. Nature 1976, 261 (5559), 403−404.

(44) Cahen, D.; Hodes, G.; Manassen, J. S/Se Substitution in Polycrystalline CdSe Photoelectrodes: Photoelectrochemical Energy Conversion. J. Electrochem. Soc. 1978, 125 (10), 1623−1628.

(45) Tenne, R.; Hodes, G. Improved Efficiency of CdSe Photo-anodes by Photoelectrochemical Etching. Appl. Phys. Lett. 1980, 37 (4), 428−430.

(46) Skotheim, T. A.; Inganas, O. Polymer Solid Electrolyte Photoelectrochemical Cells with N-Si-Polypyrrole Photoelectrodes. J. Electrochem. Soc. 1985, 132 (9), 2116−2120.

(47) Licht, S.; Peramunage, D. Rational Electrolyte Modification of n - CdSe/([KFe (CN) 6] 3 − /2 −) Photoelectrochemistry. J. Electrochem. Soc. 1992, 139 (2), L23−L26.

(48) Hada, H.; Takaoka, K.; Saikawa, M.; Yonezawa, Y. Energy Conversion and Storage in Solid-State Photogalvanic Cells. Bull. Chem. Soc. Jpn. 1981, 54 (6), 1640−1644.

(49) Yonezawa, Y.; Okai, M.; Ishino, M.; Hada, H. A Photochemical Storage Battery with an n -GaP Photoelectrode. Bull. Chem. Soc. Jpn. 1983, 56 (10), 2873−2876.

(50) Sharon, M.; Tamizhmani, G. Transition Metal Phosphide Semiconductors for Their Possible Use in Photoelectrochemical Cells and Solar Chargeable Battery (Saur Viddyut Kosh V). J. Mater. Sci. 1986, 21 (6), 2193−2201.

(51) Betz, G.; Fiechter, S.; Tributsch, H. Photon Energy Conversion and Storage with a Light-driven Insertion Reaction. J. Appl. Phys. 1987, 62 (11), 4597−4605.

(52) KANBARA, T.; TAKADA, K.; YAMAMURA, Y.; KONDO, S. Photo-Rechargeable Solid State Battery. Solid State Ionics 1990, 40−41, 955−958.

(53) Nomiyama, T.; Kuriyaki, H.; Hirakawa, K. Photo-Rechargeable Battery Using New Layer Compound CuFeTe2. Synth. Met. 1995, 71 (1−3), 2237−2238.

(54) Zou, X.; Maesako, N.; Nomiyama, T.; Horie, Y.; Miyazaki, T. Photo-Rechargeable Battery with TiO2/Carbon Fiber Electrodes Prepared by Laser Deposition. Sol. Energy Mater. Sol. Cells 2000, 62 (1−2), 133−142.

(55) Lee, A.; Vörös, M.; Dose, W. M.; Niklas, J.; Poluektov, O.; Schaller, R. D.; Iddir, H.; Maroni, V. A.; Lee, E.; Ingram, B.; Curtiss, L. A.; Johnson, C. S. Photo-Accelerated Fast Charging of Lithium-Ion Batteries. Nat. Commun. 2019, 10 (1), 4946.

(56) Tributsch, H. Photo-Intercalation: Possible Application in Solar Energy Devices. Appl. Phys. 1980, 23 (1), 61−71.

(57) Hauch, A.; Georg, A.; Krasŏ vec, U. O.; Orel, B. Photovoltaically Self-Charging Battery. J. Electrochem. Soc. 2002, 149 (9), A1208.

(58) Boruah, B. D.; Mathieson, A.; Wen, B.; Jo, C.; Deschler, F.; De Volder, M. Photo-Rechargeable Zinc-Ion Capacitor Using 2D Graphitic Carbon Nitride. Nano Lett. 2020, 20 (8), 5967−5974.

(59) Boruah, B. D.; Wen, B.; Nagane, S.; Zhang, X.; Stranks, S. D.; Boies, A.; De Volder, M. Photo-Rechargeable Zinc-Ion Capacitors Using V 2 O 5 -Activated Carbon Electrodes. ACS Energy Lett. 2020, 5 (10), 3132−3139.

(60) Liu, Y.; Li, N.; Wu, S.; Liao, K.; Zhu, K.; Yi, J.; Zhou, H. Reducing the Charging Voltage of a Li−O 2 Battery to 1.9 V by Incorporating a Photocatalyst. Energy Environ. Sci. 2015, 8 (9), 2664−2667.

(61) Yan, N. F.; Li, G. R.; Gao, X. P. Solar Rechargeable Redox Flow Battery Based on Li2WO4/LiI Couples in Dual-Phase Electrolytes. J. Mater. Chem. A 2013, 1 (24), 7012.

(62) Law, M.; Greene, L. E.; Johnson, J. C.; Saykally, R.; Yang, P. Nanowire Dye-Sensitized Solar Cells. Nat. Mater. 2005, 4 (6), 455−459.

(63) Kuang, D.; Brillet, J.; Chen, P.; Takata, M.; Uchida, S.; Miura, H.; Sumioka, K.; Zakeeruddin, S. M.; Grätzel, M. Application of Highly Ordered TiO 2 Nanotube Arrays in Flexible Dye-Sensitized Solar Cells. ACS Nano 2008, 2 (6), 1113−1116.

(64) Varghese, O. K.; Paulose, M.; Grimes, C. A. Long Vertically Aligned Titania Nanotubes on Transparent Conducting Oxide for Highly Efficient Solar Cells. Nat. Nanotechnol. 2009, 4 (9), 592−597.

(65) Kalyanasundaram, E. K.; Bertoz, M.; Bisquert, J.; De Angelis, F.; Desilvestro, H.; Fabregat-santiago, F.; Fantacci, S.; Hagfeldt, A.; Ito, S.; Jiang, K.; Kalyanasundaram, K.; Kamat, P. V; Kavan, L.; Moser, J.; Nazeeruddin, K.; Peter, L.; Snaith, H. J.; Tulloch, G.; Tulloch, S.; Uchida, S.; Yanagida, S.; Yum, J. Dye-Sensitized Solar Cells; EPLF Press: 2010.

(66) Kim, B.-M.; Lee, M.-H.; Dilimon, V. S.; Kim, J. S.; Nam, J. S.; Cho, Y.-G.; Noh, H. K.; Roh, D.-H.; Kwon, T.-H.; Song, H.-K. Indoor-Light-Energy-Harvesting Dye-Sensitized Photo-Rechargeable Battery. Energy Environ. Sci. 2020, 13 (5), 1473−1480.

(67) Yan, N. F.; Li, G. R.; Pan, G. L.; Gao, X. P. TiN Nanotube Arrays as Electrocatalytic Electrode for Solar Storable Rechargeable Battery. J. Electrochem. Soc. 2012, 159 (11), A1770−A1774.

(68) Zhang, X.; Huang, X.; Li, C.; Jiang, H. Dye-Sensitized Solar Cell with Energy Storage Function through PVDF/ZnO Nano-composite Counter Electrode. Adv. Mater. 2013, 25 (30), 4093−4096.

(69) Zhang, W.; Eperon, G. E.; Snaith, H. J. Metal Halide Perovskites for Energy Applications. Nat. Energy 2016, 1 (6), 16048.

(70) Zhang, X.; Song, W.; Tu, J.; Wang, J.; Wang, M.; Jiao, S. A Review of Integrated Systems Based on Perovskite Solar Cells and Energy Storage Units: Fundamental, Progresses, Challenges, and Perspectives. Adv. Sci. 2021, 8 (14), 2100552.

(71) Pham, H. D.; Yang, T. C.; Jain, S. M.; Wilson, G. J.; Sonar, P. Development of Dopant-Free Organic Hole Transporting Materials for Perovskite Solar Cells. Adv. Energy Mater. 2020, 10 (13), 1903326.

(72) Dong, Q.; Fang, Y.; Shao, Y.; Mulligan, P.; Qiu, J.; Cao, L.; Huang, J. Electron-Hole Diffusion Lengths > 175 Mm in Solution-Grown CH 3 NH 3 PbI 3 Single Crystals. Science (80-.) 2015, 347 (6225), 967−970.

(73) Giovanni, D.; Righetto, M.; Zhang, Q.; Lim, J. W. M.; Ramesh, S.; Sum, T. C. Origins of the Long-Range Exciton Diffusion in Perovskite Nanocrystal Films: Photon Recycling vs Exciton Hopping. Light Sci. Appl. 2021, 10 (1), 2.

(74) Yoo, J. J.; Seo, G.; Chua, M. R.; Park, T. G.; Lu, Y.; Rotermund, F.; Kim, Y. K.; Moon, C. S.; Jeon, N. J.; Correa-Baena, J. P.; Bulović, V.; Shin, S. S.; Bawendi, M. G.; Seo, J. Efficient Perovskite Solar Cells via Improved Carrier Management. Nature 2021, 590 (7847), 587− 1499 593.

(75) Tammireddy, S.; Reichert, S.; An, Q.; Taylor, A. D.; Ji, R.; Paulus, F.; Vaynzof, Y.; Deibel, C. Temperature-Dependent Ionic Conductivity and Properties of Iodine-Related Defects in Metal Halide Perovskites. ACS Energy Lett. 2022, 7 (1), 310−319.

(76) Zhu, Z.; Kushima, A.; Yin, Z.; Qi, L.; Amine, K.; Lu, J.; Li, J. Anion-Redox Nanolithia Cathodes for Li-Ion Batteries. Nat. Energy 2016, 1 (8), 16111.

(77) Read, J.; Mutolo, K.; Ervin, M.; Behl, W.; Wolfenstine, J.; Driedger, A.; Foster, D. Oxygen Transport Properties of Organic Electrolytes and Performance of Lithium/Oxygen Battery. J. Electrochem. Soc. 2003, 150 (10), A1351. 1511

(78) Dong, Y.; Zou, Y.; Song, J.; Song, X.; Zeng, H. Recent Progress of Metal Halide Perovskite Photodetectors. J. Mater. Chem. C 2017, 5 (44), 11369−11394.

(79) Baranowski, M.; Plochocka, P. Excitons in Metal-Halide Perovskites. Adv. Energy Mater. 2020, 10 (26), 1903659.

(80) Yang, J. M.; Luo, Y.; Bao, Q.; Li, Y. Q.; Tang, J. X. Recent Advances in Energetics and Stability of Metal Halide Perovskites for Optoelectronic Applications. Adv. Mater. Interfaces 2019, 6 (3), 1801351.

(81) Ahmad, S.; Sadhanala, A.; Hoye, R. L. Z.; Andrei, V.; Modarres, M. H.; Zhao, B.; Rongé, J.; Friend, R.; De Volder, M. Triple-Cation-Based Perovskite Photocathodes with AZO Protective Layer for Hydrogen Production Applications. ACS Appl. Mater. Interfaces 2019, 11 (26), 23198−23206.

(82) Ni, L.; Huynh, U.; Cheminal, A.; Thomas, T. H.; Shivanna, R.; Hinrichsen, T. F.; Ahmad, S.; Sadhanala, A.; Rao, A. Real-Time Observation of Exciton-Phonon Coupling Dynamics in Self-Assembled Hybrid Perovskite Quantum Wells. ACS Nano 2017, 11 (11), 10834−10843.

(83) Ahmad, S.; Kanaujia, P. K.; Niu, W.; Baumberg, J. J.; Vijaya Prakash, G. In Situ Intercalation Dynamics in Inorganic−Organic Layered Perovskite Thin Films. ACS Appl. Mater. Interfaces 2014, 6 (13), 10238−10247.

(84) Sadhanala, A.; Ahmad, S.; Zhao, B.; Giesbrecht, N.; Pearce, P. M.; Deschler, F.; Hoye, R. L. Z.; Gödel, K. C.; Bein, T.; Docampo, P.; Dutton, S. E.; De Volder, M. F. L.; Friend, R. H. Blue-Green Color Tunable Solution Processable Organolead Chloride−Bromide Mixed Halide Perovskites for Optoelectronic Applications. Nano Lett. 2015, 15 (9), 6095−6101.

(85) Rahil, M.; Rajput, P.; Ghosh, D.; Ahmad, S. Highly Tunable Single-Phase Excitons in Mixed Halide Layered Perovskites. ACS Appl. Electron. Mater. 2020, 2 (10), 3199−3210.

(86) Andrei, V.; Hoye, R. L. Z.; Crespo-Quesada, M.; Bajada, M.; Ahmad, S.; De Volder, M.; Friend, R.; Reisner, E. Scalable Triple Cation Mixed Halide Perovskite−BiVO4 Tandems for Bias-Free Water Splitting. Adv. Energy Mater. 2018, 8 (25), 1801403.

(87) Rahil, M.; Mushtaq, N.; Ansari, H. R.; Alam, M. K.; Ahmad, S. Exciton Tunability in Mixed Halide Hybrid Layered Perovskites. AIP Conf. Proc. 2019, 2276, 020043.

(88) Ahmad, S.; Kanaujia, P. K.; Beeson, H. J.; Abate, A.; Deschler, F.; Credgington, D.; Steiner, U.; Prakash, G. V.; Baumberg, J. J. Strong Photocurrent from Two-Dimensional Excitons in Solution-Processed Stacked Perovskite Semiconductor Sheets. ACS Appl. Mater. Interfaces 2015, 7 (45), 25227−25236.

(89) Ahmad, S.; Baumberg, J. J.; Vijaya Prakash, G. Structural Tunability and Switchable Exciton Emission in Inorganic-Organic Hybrids with Mixed Halides. J. Appl. Phys. 2013, 114 (23), 233511.

(90) Saikumar, I.; Ahmad, S.; Baumberg, J. J.; Vijaya Prakash, G. Fabrication of Excitonic Luminescent Inorganic−Organic Hybrid Nano- and Microcrystals. Scr. Mater. 2012, 67 (10), 834−837.

(91) Ahmad, S.; Prakash, G. V. Strong Room-Temperature Ultraviolet to Red Excitons from Inorganic Organic-Layered Perovskites, (R-NH3)2MX4 (M = Pb2+, Sn2+, Hg2+; X = I−, Br−). J. Nanophotonics 2014, 8 (1), 083892.

(92) Ahmad, S.; Hanmandlu, C.; Kanaujia, P. K.; Prakash, G. V. Direct Deposition Strategy for Highly Ordered Inorganic Organic Perovskite Thin Films and Their Optoelectronic Applications. Opt. Mater. Express 2014, 4 (7), 1313.

(93) Ahmad, S.; Prakash, G. V. Two-Step Fabrication of R-PbI_4(1-y)Br_4y Type Light Emitting Inorganic-Organic Hybrid Photonic Structures. Opt. Mater. Express 2014, 4 (1), 101.

(94) Rahil, M.; Ansari, R. M.; Prakash, C.; Islam, S. S.; Dixit, A.; Ahmad, S. Ruddlesden−Popper 2D Perovskites of Type (C6H9C2H4NH3)2(CH3NH3)N−1PbnI3n+1 (n = 1−4) for Optoelectronic Applications. Sci. Rep. 2022, 12 (1), 2176.

(95) Dawson, J. A.; Naylor, A. J.; Eames, C.; Roberts, M.; Zhang, W.; Snaith, H. J.; Bruce, P. G.; Saiful Islam, M. Mechanisms of Lithium Intercalation and Conversion Processes in Organic-Inorganic Halide Perovskites. ACS Energy Lett. 2017, 2 (8), 1818−1824.

(96) Xia, H.-R.; Sun, W.-T.; Peng, L.-M. Hydrothermal Synthesis of Organometal Halide Perovskites for Li-Ion Batteries. Chem. Commun. 2015, 51 (72), 13787−13790.

(97) Vicente, N.; Garcia-Belmonte, G. Methylammonium Lead Bromide Perovskite Battery Anodes Reversibly Host High Li-Ion Concentrations. J. Phys. Chem. Lett. 2017, 8 (7), 1371−1374.

(98) Vicente, N.; Garcia-Belmonte, G. Organohalide Perovskites Are Fast Ionic Conductors. Adv. Energy Mater. 2017, 7 (19), 1700710.

(99) He, M.; Zhang, L.; Li, J. Theoretical Investigation on Interactions between Lithium Ions and Two-Dimensional Halide Perovskite for Solar-Rechargeable Batteries. Appl. Surf. Sci. 2021, 541, 148509.

(100) Wang, Q.; Yang, T.; Wang, H.; Zhang, J.; Guo, X.; Yang, Z.; Lu, S.; Qin, W. Morphological and Chemical Tuning of Lead Halide Perovskite Mesocrystals as Long-Life Anode Materials in Lithium-Ion Batteries. CrystEngComm 2019, 21 (6), 1048−1059.

(101) Mathieson, A.; Rahil, M.; Zhang, Y.; Dose, W. M.; Lee, J. T.; Deschler, F.; Ahmad, S.; De Volder, M. Ruddlesden Popper 2D Perovskites as Li-Ion Battery Electrodes. Mater. Adv. 2021, 2 (10), 3370−3377.

(102) Liu, S.; Kang, L.; Kim, J. M.; Chun, Y. T.; Zhang, J.; Jun, S. C. Recent Advances in Vanadium-Based Aqueous Rechargeable Zinc-Ion Batteries. Adv. Energy Mater. 2020, 10 (25), 2000477.

(103) Yao, J.; Li, Y.; Massé, R. C.; Uchaker, E.; Cao, G. Revitalized Interest in Vanadium Pentoxide as Cathode Material for Lithium-Ion Batteries and Beyond. Energy Storage Mater. 2018, 11, 205−259.

(104) Saravanan, R.; Gupta, V. K.; Mosquera, E.; Gracia, F. Preparation and Characterization of V2O5/ZnO Nanocomposite System for Photocatalytic Application. J. Mol. Liq. 2014, 198, 409−412.

(105) Margoni, M. M.; Mathuri, S.; Ramamurthi, K.; Babu, R. R.; Sethuraman, K. Investigation on the Pure and Fluorine Doped Vanadium Oxide Thin Films Deposited by Spray Pyrolysis Method. Thin Solid Films 2016, 606, 51−56.

(106) Margoni, M. M.; Mathuri, S.; Ramamurthi, K.; Babu, R. R.; Sethuraman, K. Sprayed Vanadium Pentoxide Thin Films: Influence of Substrate Temperature and Role of HNO3 on the Structural, Optical, Morphological and Electrical Properties. Appl. Surf. Sci. 2017, 418, 280−290.

(107) Boruah, B. D.; Wen, B.; Nagane, S.; Zhang, X.; Stranks, S. D.; Boies, A.; De Volder, M. Photo-Rechargeable Zinc-Ion Capacitors Using V2O5-Activated Carbon Electrodes. ACS Energy Lett. 2020, 5 (10), 3132−3139.

(108) Wu, G.; Du, K.; Xia, C.; Kun, X.; Shen, J.; Zhou, B.; Wang, J. Optical Absorption Edge Evolution of Vanadium Pentoxide Films during Lithium Intercalation. Thin Solid Films 2005, 485 (1−2), 284−289.

(109) Wang, Q.; Brier, M.; Joshi, S.; Puntambekar, A.; Chakrapani, V. Defect-Induced Burstein-Moss Shift in Reduced V2O5 Nanostructures. Phys. Rev. B 2016, 94 (24), 245305.

(110) Wang, J.; Wang, Y.; Zhu, C.; Liu, B. Photoinduced Rechargeable Lithium-Ion Battery. ACS Appl. Mater. Interfaces 2022, 14 (3), 4071−4078.

(111) Martinez, S.; Sobrados, I.; Tonti, D.; Amarilla, J. M.; Sanz, J. Chemical vs. Electrochemical Extraction of Lithium from the Li-Excess Li1.10Mn1.90O4 Spinel Followed by NMR and DRX Techniques. Phys. Chem. Chem. Phys. 2014, 16 (7), 3282.

(112) Scivetti, I.; Teobaldi, G. (Sub)Surface-Promoted Disproportionation and Absolute Band Alignment in High-Power LiMn 2 O 4 Cathodes. J. Phys. Chem. C 2015, 119 (37), 21358−21368.

(113) Zhan, C.; Lu, J.; Jeremy Kropf, A.; Wu, T.; Jansen, A. N.; Sun, Y.-K.; Qiu, X.; Amine, K. Mn(II) Deposition on Anodes and Its Effects on Capacity Fade in Spinel Lithium Manganate−Carbon Systems. Nat. Commun. 2013, 4 (1), 2437.

(114) Amos, C. D.; Roldan, M. A.; Varela, M.; Goodenough, J. B.; Ferreira, P. J. Revealing the Reconstructed Surface of Li[Mn 2]O 4. Nano Lett. 2016, 16 (5), 2899−2906.

(115) Ohzuku, T.; Kitagawa, M.; Hirai, T. Electrochemistry of Manganese Dioxide in Lithium Nonaqueous Cell: I. X-Ray Diffractional Study on the Reduction of Electrolytic Manganese Dioxide. J. Electrochem. Soc. 1989, 136 (11), 3169−3174.

(116) Miroshnikov, M.; Kato, K.; Babu, G.; Divya, K. P.; Reddy Arava, L. M.; Ajayan, P. M.; John, G. A Common Tattoo Chemical for Energy Storage: Henna Plant-Derived Naphthoquinone Dimer as a Green and Sustainable Cathode Material for Li-Ion Batteries. RSC Adv. 2018, 8 (3), 1576−1582.

(117) Miroshnikov, M.; Kato, K.; Babu, G.; Thangavel, N. K.; Mahankali, K.; Hohenstein, E.; Wang, H.; Satapathy, S.; Divya, K. P.; Asare, H.; Ajayan, P. M.; Arava, L. M. R.; John, G. Made From Henna! A Fast-Charging, High-Capacity, and Recyclable Tetrakislaw-sone Cathode Material for Lithium Ion Batteries. ACS Sustain. Chem. Eng. 2019, 7 (16), 13836−13844.

(118) Lee, J.; Park, M. J. Tattooing Dye as a Green Electrode Material for Lithium Batteries. Adv. Energy Mater. 2017, 7 (12), 1602279.

(119) Khadtare, S. S.; Ware, A. P.; Salunke-Gawali, S.; Jadkar, S. R.; Pingale, S. S.; Pathan, H. M. Dye Sensitized Solar Cell with Lawsone Dye Using a ZnO Photoanode: Experimental and TD-DFT Study. RSC Adv. 2015, 5 (23), 17647−17652.

(120) Hu, C.; Chen, L.; Hu, Y.; Chen, A.; Chen, L.; Jiang, H.; Li, C. Light-Motivated SnO 2 /TiO 2 Heterojunctions Enabling the Breakthrough in Energy Density for Lithium-Ion Batteries. Adv. Mater. 2021, 33 (49), 2103558.

(121) Kumar, A.; Thakur, P.; Sharma, R.; Puthirath, A. B.; Ajayan, P. M.; Narayanan, T. N. Photo Rechargeable Li-Ion Batteries Using Nanorod Heterostructure Electrodes. Small 2021, 17 (51), 2105029.

(122) Bouteau, G.; Van-Nhien, A. N.; Sliwa, M.; Sergent, N.; Lepretre, J.-C.; Gachot, G.; Sagaidak, I.; Sauvage, F. Effect of Standard Light Illumination on Electrolyte's Stability of Lithium-Ion Batteries Based on Ethylene and Di-Methyl Carbonates. Sci. Rep. 2019, 9 (1), 135.